Inorganic Chemistry

ARTICLE

pubs.acs.org/IC

Synthesis, Crystal Structures, and Magnetic Properties of a New Family of Heterometallic Cyanide-Bridged $Fe^{III}_2M^{II}_2$ (M = Mn, Ni, and Co) Square Complexes

Emilio Pardo,*[†] Michel Verdaguer,[†] Patrick Herson,[†] Helene Rousselière,[†] Joan Cano,[‡] Miguel Julve,[‡] Francesc Lloret,[‡] and Rodrigue Lescouëzec*[†]

[†]Institut Parisien de Chimie Moléculaire, Université Pierre et Marie Curie-Paris 6, UMR 7201, F-75252 Paris, France

[‡]Departament de Química Inorgànica, Instituto de Ciencia Molecular (ICMOL), Universitat de València, 46980 Paterna, València, Spain

Supporting Information

ABSTRACT: New heterobimetallic tetranuclear complexes of formula $[Fe^{III}\{B(pz)_4\}(CN)_2(\mu\text{-}CN)Mn^{II}(bpy)_2]_2(ClO_4)_2\cdot CH_3CN$ (**1**), $[Fe^{III}\{HB(pz)_3\}(CN)_2(\mu\text{-}CN)Ni^{II}(dmphen)_2]_2(ClO_4)_2\cdot 2CH_3OH$ (**2a**), $[Fe^{III}\{B(pz)_4\}(CN)_2(\mu\text{-}CN)Ni^{II}(dmphen)_2]_2(ClO_4)_2\cdot 2CH_3OH$ (**2b**), $[Fe^{III}\{HB(pz)_3\}(CN)_2(\mu\text{-}CN)Co^{II}(dmphen)_2]_2(ClO_4)_2\cdot 2CH_3OH$ (**3a**), and $[Fe^{III}\{B(pz)_4\}(CN)_2(\mu\text{-}CN)Co^{II}(dmphen)_2]_2(ClO_4)_2\cdot 2CH_3OH$ (**3b**), [$HB(pz)_3^-$ = hydrotris(1-pyrazolyl)borate, $B(Pz)_4^-$ = tetrakis(1-pyrazolyl)borate, dmphen = 2,9-dimethyl-1,10-phenanthroline, bpy = 2,2′-bipyridine] have been synthesized and structurally and magnetically characterized. Complexes **1**−**3b** have been prepared by following a rational route based on the self-assembly of the tricyanometalate precursor *fac*-$[Fe^{III}(L)(CN)_3]^-$ (L = tridentate anionic ligand) and cationic preformed complexes $[M^{II}(L')_2(H_2O)_2]^{2+}$ (L′ = bidentate α-diimine type ligand), this last species having four blocked coordination sites and two labile ones located in cis positions. The structures of **1**−**3b** consist of cationic tetranuclear $Fe^{III}_2M^{II}_2$ square complexes [M = Mn (**1**), Ni (**2a** and **2b**), Co (**3a** and **3b**)] where corners are defined by the metal ions and the edges by the Fe−CN−M units. The charge is balanced by free perchlorate anions. The $[Fe(L)(CN)_3]^-$ complex in **1**−**3b** acts as a ligand through two cyanide groups toward two divalent metal complexes. The magnetic properties of **1**−**3b** have been investigated in the temperature range 2−300 K. A moderately strong antiferromagnetic interaction between the low-spin Fe^{III} ($S = 1/2$) and high-spin Mn^{II} ($S = 5/2$) ions has been found for **1** leading to an $S = 4$ ground state ($J_1 = -6.2$ and $J_2 = -2.7$ cm^{-1}), whereas a moderately strong ferromagnetic interaction between the low-spin Fe^{III} ($S = 1/2$) and high-spin Ni^{II} ($S = 1$) and Co^{II} ($S = 3/2$) ions has been found for complexes **2a**−**3b** with $S = 3$ (**2a** and **2b**) and $S = 4$ (**3a** and **3b**) ground spin states [$J_1 = +21.4$ cm^{-1} and $J_2 = +19.4$ cm^{-1} (**2a**); $J_1 = +17.0$ cm^{-1} and $J_2 = +12.5$ cm^{-1} (**2b**); $J_1 = +5.4$ cm^{-1} and $J_2 = +11.1$ cm^{-1} (**3a**); $J_1 = +8.1$ cm^{-1} and $J_2 = +11.0$ cm^{-1} (**3b**)] [the exchange Hamiltonian being of the type $\hat{H} = -J(\hat{S}_i\cdot\hat{S}_j)$]. Density functional theory (DFT) calculations have been used to substantiate the nature and magnitude of the exchange magnetic coupling observed in **1**−**3b** and also to analyze the dependence of the exchange magnetic coupling on the structural parameters of the Fe−C−N−M skeleton.

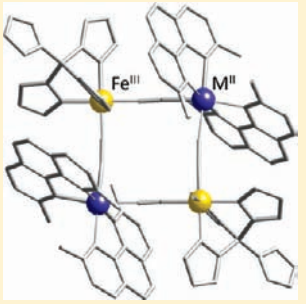

INTRODUCTION

The design of polynuclear metal complexes with predictable topology by self-assembling methods[1−5] constitutes one of the most studied subjects in coordination chemistry nowadays.[6] The topological control is indeed of outstanding interest when preparing molecular materials because their physical properties strongly depend on their architecture.[7−10] This is particularly true when dealing with magnetic properties. Among the wide variety of high-nuclearity coordination compounds with paramagnetic transition metal ions, the cyanide-bridged complexes have attracted the attention of a great number of research groups. The main reason for this interest is due to the ambidentate character of the cyanide ligand which allows the straightforward synthesis of heterometallic compounds and also its efficiency for the propagation of the exchange magnetic coupling.[11,12] Indeed, the relevance of cyanide is evidenced by the great variety of magnetic materials in which it is involved such as high-T_c molecule based magnets,[12,13] photomagnets,[14] spin crossover systems,[15] multiferroics,[16] single-molecule magnets (SMMs),[17] and single-chain magnets (SCMs).[18] Among these types of magnetic materials, the preparation of SMMs[17,19] and SCMs,[18,20] that is, compounds which exhibit slow relaxation of the magnetization below a blocking temperature (T_B),[21] has become specially relevant in recent years envisaging their potential application in molecular devices and quantum computer science.[21] The design of an SMM requires the obtention of molecules having a high-spin ground state (S) and a large negative axial magnetic anisotropy (D) which result in an energy barrier ($U = -DS^2$) for the magnetization reversal between the two lowest $m_S = \pm S$ states.[21] Thus, the synthesis of an SMM depends on the nuclearity and the topology of the polynuclear

Received: March 25, 2011
Published: June 01, 2011

assembly, as well as on the nature of the interacting metal centers and the bridging ligands.[6−9]

Recently, the so-called "complex-as-ligand/complex-as-metal" approach has been consolidated as a rational strategy toward the preparation of SMMs.[17g] This rational self-assembly method, whereby a metal complex with potential donor groups coordinates to another metal complex with partially blocked coordination sites, constitutes an appropriate route to gain control of both the nuclearity and the topology of the polymetallic species, and moreover, it allows the preparation of heteropolymetallic species.[22]

In this paper, we explore a rational self-assembly method which consists of the use of the tailored tricyanometalate precursor *fac*-$[Fe(L)(CN)_3]^-$ [L = $HB(pz)_3^-$, $B(pz)_4^-$] as trinucleating ligand toward some divalent 3d metal ions having four coordination sites blocked by α-diimine type ligands. This programmed method allows the one-step elaboration of new heterobimetallic, square tetranuclear cationic complexes of the general formula $[Fe^{III}(L)(CN)_2(\mu\text{-}CN)M^{II}(L')_2]_2^{2+}$, where the cyanide-bearing precursor coordinates two metal ions of identical nature (M = Mn^{II}, Ni^{II}, and Co^{II}) whose coordination sphere is partially blocked with two bidentate terminal ligands such as 4,4′-bipyridine (bpy) and 2,9-dimethyl-1,10-phenanthroline (dmphen) (Chart 1). Several other cyanide-bridged homo- and heterobimetallic tetranuclear squares have been reported.[14b,c,17a,23] However, only a few of them were prepared by following rational self-assembly methods through the use of blocking ligands coordinated to metal atoms in order to avoid unwanted polymerization. Here we report the preparation, crystal structures, and magnetic properties of five related tetranuclear heterobimetallic complexes of formulas $[Fe^{III}\{B(pz)_4\}(CN)_2(\mu\text{-}CN)Mn^{II}(bpy)_2]_2(ClO_4)_2\cdot CH_3CN$ (**1**), $[Fe^{III}\{HB(pz)_3\}(CN)_2(\mu\text{-}CN)Ni^{II}(dmphen)_2]_2(ClO_4)_2\cdot 2CH_3OH$ (**2a**), $[Fe^{III}\{B(pz)_4\}(CN)_2(\mu\text{-}CN)Ni^{II}(dmphen)_2]_2(ClO_4)_2\cdot 2CH_3OH$ (**2b**), $[Fe^{III}\{HB(pz)_3\}(CN)_2(\mu\text{-}CN)Co^{II}(dmphen)_2]_2(ClO_4)_2\cdot 2CH_3OH$ (**3a**), and $[Fe^{III}\{B(pz)_4\}(CN)_2(\mu\text{-}CN)Co^{II}(dmphen)_2]_2(ClO_4)_2\cdot 2CH_3OH$ (**3b**) [$HB(pz)_3^-$ = hydrotris(1-pyrazolyl) borate, $B(pz)_4^-$ = tetrakis(1-pyrazolyl)borate].

Chart 1. Heterobimetallic, Square-Type Tetranuclear Complexes

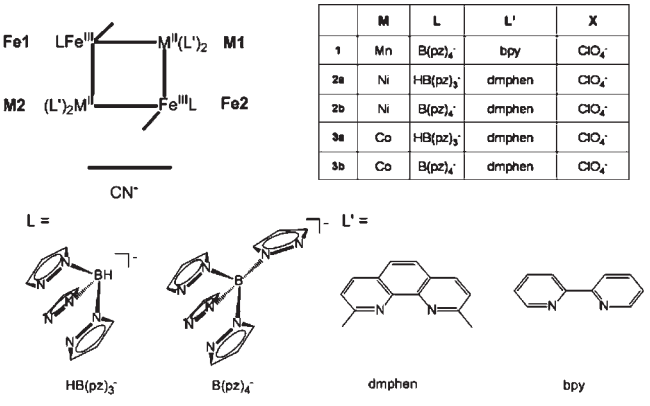

	M	L	L'	X
1	Mn	$B(pz)_4^-$	bpy	ClO_4^-
2a	Ni	$HB(pz)_3^-$	dmphen	ClO_4^-
2b	Ni	$B(pz)_4^-$	dmphen	ClO_4^-
3a	Co	$HB(pz)_3^-$	dmphen	ClO_4^-
3b	Co	$B(pz)_4^-$	dmphen	ClO_4^-

EXPERIMENTAL SECTION

General. All chemicals were of reagent grade quality, purchased from commercial sources and used as received. $PPh_4[Fe^{III}\{HB(pz)_3\}(CN)_3]\cdot H_2O$ and $PPh_4[Fe^{III}\{B(pz)_4\}(CN)_3]\cdot H_2O$ were prepared as previously reported.[24] ***Caution!*** *Cyanides are very toxic and must be handled with great caution. Waste cyanides were treated with concentrated alkaline solutions of sodium hypochlorite in order to transform the cyanide into nontoxic cyanate. Although no problem was encountered in this work, perchlorate complexes are potentially explosive and they should be handled with care. We worked at the millimole scale and heating was avoided.*

Synthesis of the Complexes $[Fe^{III}\{B(pz)_4\}(CN)_2(\mu\text{-}CN)Mn^{II}(bpy)_2]_2(ClO_4)_2\cdot CH_3CN$ (1), $[Fe^{III}\{HB(pz)_3\}(CN)_2(\mu\text{-}CN)Ni^{II}(dmphen)_2]_2(ClO_4)_2\cdot 2CH_3OH$ (2a), $[Fe^{III}\{B(pz)_4\}(CN)_2(\mu\text{-}CN)Ni^{II}(dmphen)_2]_2(ClO_4)_2\cdot 2CH_3OH$ (2b), $[Fe^{III}\{HB(pz)_3\}(CN)_2(\mu\text{-}CN)Co^{II}(dmphen)_2]_2(ClO_4)_2\cdot 2CH_3OH$ (3a), and $[Fe^{III}\{B(pz)_4\}(CN)_2(\mu\text{-}CN)Co^{II}(dmphen)_2]_2(ClO_4)_2\cdot 2CH_3OH$ (3b). Well-formed red prisms (**1** and **2a**), plates (**2b**), and needles (**3a** and **3b**) suitable for X-ray diffraction were obtained in one step by slow diffusion in an H-shaped tube of CH_3CN/H_2O (1:1) (**1**) or CH_3OH/H_2O (1:1) (**2a**−**3b**) solutions containing stoichiometric amounts (1:1) of $PPh_4[Fe^{III}(L)(CN)_3]\cdot H_2O$ and the corresponding first-row transition metal complex $[M(L')_2(S)_2](ClO_4)_2$ (M = Mn, Ni, and Co; S = solvent) previously prepared in situ from a 2:1 mixture of L′ and the corresponding perchlorate salt as hexahydrate. They were collected by filtration, washed with small amounts of CH_3CN/H_2O (1:1) (**1**) and CH_3OH/H_2O (1:1) (**2a**−**3b**), and air-dried. Satisfactory elemental analyses (C, H, N) were obtained for **1**−**3b**. The low yields observed can be explained because the slow diffusion processes were stopped prior to the formation of byproduct. Analytical and spectroscopic data are listed in Table 1.

Physical Techniques. Elemental analyses (C, H, N) were performed by the Service Interdisciplinaire d'Aide à la Recherche et à l'Enseignement (SIARE) of the UPMC University (France). IR spectra were recorded on a Perkin-Elmer 882 spectrophotometer as KBr pellets. Variable-temperature (2−300 K) magnetic susceptibility measurements were carried out on powdered samples of **1**−**3b** with a Quantum Design SQUID magnetometer. The susceptibility data were corrected for the diamagnetism of the constituent atoms and for the sample holder.

Computational Details. Calculations were performed through the Gaussian 09 package using the B3LYP functional and the quadratic convergence approach.[25] Triple-ζ and double-ζ all electron basis sets proposed by Ahlrichs et al. were used for the metal and for the rest of atoms, respectively.[26,27] The broken-symmetry approach has been employed to describe the unrestricted solutions of the antiferromagnetic spin states,[28] which have been obtained from the guess functions generated with the fragment tool implemented in Gaussian code. Full geometries have been used for **1**, **2b**, and **3b**. As noted in a previous

Table 1. Analytical and Physical Characterization Data of Complexes 1−3b[a]

complex	*M*	molecular formula	yield [%]	ν(CN) [cm^{-1}]	C [%]	H [%]	N [%]
1	1800.6	$C_{72}H_{59}B_2Cl_2Fe_2Mn_2N_{31}O_8$	21	2152, 2121	48.12 (47.98)	3.02 (3.28)	24.19 (24.10)
2a	1907.3	$C_{82}H_{76}B_2Cl_2Fe_2N_{26}Ni_2O_{10}$	34	2154, 2123	52.01 (51.59)	4.02 (3.98)	19.00 (19.08)
2b	2039.5	$C_{88}H_{80}B_2Cl_2Fe_2N_{30}Ni_2O_{10}$	42	2156, 2120	51.85 (51.78)	3.99 (3.92)	19.89 (20.59)
3a	1907.7	$C_{82}H_{76}B_2Cl_2Co_2Fe_2N_{26}O_{10}$	19	2163, 2123	51.62 (51.58)	4.02 (3.97)	19.21 (19.06)
3b	2039.7	$C_{88}H_{80}B_2Cl_2Co_2Fe_2N_{30}O_{10}$	28	2157, 2124	51.89 (51.76)	3.77 (3.91)	20.71 (20.56)

[a] The calculated values of elemental analysis are given in parentheses.

dx.doi.org/10.1021/ic200616p |*Inorg. Chem.* 2011, 50, 6250–6262

report,[29] there are some problems in certain cases to reaching the imposed convergence criterion or the well-found electronic configuration is not adequate for the ground spin state. This fact is usual in systems containing cobalt(II) ions with strong spin−orbit coupling.[29] Another reason for this is that there are negative charged cyanide groups close to largely positive charges from the metal ions, with such a feature leading to an unstable situation.[30] Even though it looks like the experimental molecule, in the last case the tetranuclear molecules are not isolated and they are connected with other molecules by means of hydrogen bonds involving terminal cyanide groups. Thus, these interactions partially remove the electronic density surplus on the peripheral cyanide groups causing (i) a stabilization of the system and (ii) a decrease of the ligand field strength of the cyanide group. In this sense, we could also consider the external molecules (simplified fragments) that are involved in hydrogen bonding with the tetranuclear complexes or, alternatively, put the magnetically coupled complexes into a cavity with a dielectric constant that simulates the electronic effects of polar solvent molecules or of other molecules in the solid that are placed around it. The usual calculations and other ones introducing the mentioned approaches have been done on the $Fe^{III}_2Ni^{II}_2$ complex (**2b**). Because the calculations are slow enough due to the large size of the systems, only the approach that includes a cavity with a dielectric constant has been considered for those with more problems to reach the convergence criterion [Fe_2Mn_2 (**1**) and Fe_2Co_2 (**3b**)]. In this approach, we used a polarizable continuum model with the parameters corresponding to the acetonitrile solvent.[31] For the $Fe^{III}_2Ni^{II}_2$ system (**2b**), very close results were found with the normal calculations and other approaches. In order to simplify the discussion, only the results obtained from the approach that is common in all cases have been shown in Table 9. This kind of approach allowed reaching the electronic spin configuration in each case, but even though the computational time was significantly reduced, the process was still slow.

The broken-symmetry methodology also allows estimating all the exchange coupling constants that are present in polynuclear transition metal complexes. In order to calculate the n J_i exchange coupling constants of a polynuclear complex, we must perform at least $n + 1$ energy calculations of different spin configurations that correspond to single-determinant Kohn−Sham solutions. The spin configurations must be selected in such way that it is possible to solve a system of n equations with n unknowns, i.e., the J_i values. In this way, three calculations are needed for each of the complexes **1**, **2b**, and **3b** in order to obtain the two exchange coupling constants (see Table 9). One additional electronic configuration has been calculated to avoid possible errors or lacks in the computational procedure. The values of the J_i constants are obtained by a fit process from the energies of the following spin configurations: a high-spin state where all the local spin moments are parallel, singlet spin states where the local spin moments of the Fe−M units are opposed to each other, and electronic configurations where the spin local moments on the iron(III) ions are antiparallel with those on the divalent metal ions.

Crystal Structure Data Collection and Refinement. Intensity data of **1**−**3b** were collected with a Bruker-Nonius KappaCCD diffractometer with graphite-monochromated Mo Kα radiation. Unit cell parameter determination, data collection strategy, and integration were carried out with the Nonius EVAL-14 suite of programs.[32a] Multiscan absorption correction was applied.[32b] The structures of **1**−**3b** were solved by direct methods and refined with full-matrix least-squares technique on F^2 using the SIR 92,[32c] Superflip,[32d] SHELXL-97,[32e] and CRYSTAL programs.[32f] Data collection and data reduction were done with the COLLECT[32g] and EVALCCD[32a] programs. All calculations for data reduction, structure solution, and refinement were carried out by standard procedures (CRYSTAL and WINGX).[32h] The final geometric calculations and the graphic manipulations were performed with the PLATON[32i] and CRYSTAL MAKER[32j] programs. Hydrogen atoms were introduced at calculated positions (and their coordinates were refined with an overall isotropic thermal parameter), while those of the solvent molecules were neither found nor calculated except for one methanol molecule. A summary of the crystallographic data for **1**−**3b** are given in Table 2, and selected bond distances and angles for **1**−**3b** are listed in Tables 3−7.

RESULTS AND DISCUSSION

Cyanide is a well-known ligand in molecular magnetic studies because of its remarkable ability to mediate strong magnetic

Table 2. Summary of Crystallographic Data for 1−3b

	1	2a	2b	3a	3b
formula	$C_{72}H_{59}B_2Cl_2Fe_2Mn_2N_{31}O_8$	$C_{82}H_{76}B_2Cl_2Fe_2N_{26}Ni_2O_{10}$	$C_{88}H_{80}B_2Cl_2Fe_2N_{30}Ni_2O_{10}$	$C_{82}H_{68}B_2Cl_2Co_2Fe_2N_{26}O_{10}$	$C_{88}H_{72}B_2Cl_2Co_2Fe_2N_{30}O_{10}$
M (g mol^{-1})	1800.60	1907.32	2039.46	1899.70	2031.82
crystal system	triclinic	triclinic	monoclinic	triclinic	monoclinic
space group	$P\bar{1}$	$P\bar{1}$	$P2_1/c$	$P\bar{1}$	$P2_1/c$
a (Å)	12.9622(16)	11.3380(12)	15.137(2)	11.410(2)	15.133(3)
b (Å)	13.457(2)	13.754(2)	20.493(3)	13.855(4)	20.446(6)
c (Å)	13.9192(13)	15.156(2)	15.538(2)	15.160(28)	15.613(3)
α (deg)	84.982(11)	96.717(14)	90.0	97.67(3)	90.0
β (deg)	75.157(12)	104.190(8)	106.368(8)	104.08(5)	106.244(14)
γ (deg)	61.981(11)	106.028(10)	90.0	105.24(5)	90.0
V (Å^3)	2070.4(5)	2158.7(5)	4624.9(11)	2192.4(2)	4637.6(18)
Z	1	1	2	1	2
ρ_{calc} (g cm^{-3})	1.444	1.467	1.465	1.439	1.455
$F(000)$	918	982	2100	972	2080
μ (mm^{-1})	0.779	0.895	0.842	0.830	0.791
T (K)	200(2)	200(2)	200(2)	200(2)	200(2)
R^a [$I > 2\sigma(I)$]	0.0484	0.0485	0.0476	0.0693	0.0648
wR^b [$I > 2\sigma(I)$]	0.1372	0.1342	0.1373	0.1720	0.2130
S^c	1.054	1.023	1.057	0.9769	1.156

[a] $R = \Sigma(|F_o| - |F_c|)/\Sigma|F_o|$. [b] $wR = [\Sigma w(|F_o| - |F_c|)^2/\Sigma w|F_o|^2]^{1/2}$. [c] $S = [\Sigma w(|F_o| - |F_c|)^2/(N_o - N_p)]^{1/2}$.

dx.doi.org/10.1021/ic200616p |Inorg. Chem. 2011, 50, 6250–6262

Table 3. Selected Bond Distances (Å) and Angles (deg) for 1[a,b]

Mn(1)−N(1)′	2.192(3)	Mn(1)−N(2)	2.196(2)
Mn(1)−N(10)	2.327(2)	Mn(1)−N(11)	2.263(2)
Mn(1)−N(12)	2.272(2)	Mn(1)−N(13)	2.292(2)
Fe(1)−C(1)	1.931(3)	Fe(1)−C(2)	1.942(3)
Fe(1)−C(3)	1.938(3)	Fe(1)−N(4)	1.989(2)
Fe(1)−N(6)	1.984(2)	Fe(1)−N(8)	1.983(2)
N(1)′−Mn(1)−N(2)	90.15(9)	N(1)′−Mn(1)−N(10)	89.04(9)
N(2)−Mn(1)−N(10)	173.80(9)	N(1)′−Mn(1)−N(11)	100.22(10)
N(2)−Mn(1)−N(11)	102.07(9)	N(10)−Mn(1)−N(11)	72.04(9)
N(1)′−Mn(1)−N(12)	94.17(10)	N(2)−Mn(1)−N(12)	96.73(9)
N(10)−Mn(1)−N(12)	89.46(9)	N(11)−Mn(1)−N(12)	156.18(9)
N(1)′−Mn(1)−N(13)	166.15(9)	N(2)−Mn(1)−N(13)	94.88(9)
N(10)−Mn(1)−N(13)	87.31(8)	N(11)−Mn(1)−N(13)	91.35(9)
N(12)−Mn(1)−N(13)	72.45(9)	C(1)−Fe(1)−C(2)	90.38(11)
C(1)−Fe(1)−C(3)	86.01(12)	C(2)−Fe(1)−C(3)	86.90(11)
C(1)−Fe(1)−N(4)	177.62(10)	C(2)−Fe(1)−N(4)	91.79(10)
C(3)−Fe(1)−N(4)	93.13(11)	C(1)−Fe(1)−N(6)	90.53(10)
C(2)−Fe(1)−N(6)	178.92(11)	C(3)−Fe(1)−N(6)	92.58(10)
N(4)−Fe(1)−N(6)	87.29(9)	C(1)−Fe(1)−N(8)	91.65(11)
C(2)−Fe(1)−N(8)	92.65(10)	C(3)−Fe(1)−N(8)	177.62(11)
N(4)−Fe(1)−N(8)	89.23(9)	N(6)−Fe(1)−N(8)	87.90(9)

[a] The estimated standard deviations are given in parentheses. [b] Symmetry code: (′) = 1 − *x*, 1 − *y*, 1 − *z*.

Table 4. Selected Bond Distances (Å) and Angles (deg) for 2a[a,b]

Ni(1)−N(1)	2.102(2)	Ni(1)−N(2)	2.098(2)
Ni(1)−N(10)	2.152(2)	Ni(1)−N(11)	2.164(2)
Ni(1)−N(12)	2.134(2)	Ni(1)−N(13)	2.157(2)
Fe(1)−C(1)	1.941(3)	Fe(1)−C(2)′	1.935(3)
Fe(1)−C(3)	1.949(3)	Fe(1)−N(4)	1.996(2)
Fe(1)−N(6)	2.001(2)	Fe(1)−N(8)	1.975(2)
N(1)−Ni(1)−N(2)	86.58(8)	N(1)−Ni(1)−N(10)	174.66(8)
N(2)−Ni(1)−N(10)	90.13(8)	N(1)−Ni(1)−N(11)	96.88(8)
N(2)−Ni(1)−N(11)	81.07(8)	N(10)−Ni(1)−N(11)	78.43(8)
N(1)−Ni(1)−N(12)	86.17(8)	N(2)−Ni(1)−N(12)	172.27(8)
N(10)−Ni(1)−N(12)	97.29(8)	N(11)−Ni(1)−N(12)	102.46(8)
N(1)−Ni(1)−N(13)	84.77(8)	N(2)−Ni(1)−N(13)	97.50(8)
N(10)−Ni(1)−N(13)	99.85(8)	N(11)−Ni(1)−N(13)	177.73(8)
N(12)−Ni(1)−N(13)	79.17(8)	C(1)−Fe(1)−C(2)′	88.26(10)
C(1)−Fe(1)−C(3)	90.02(10)	C(2)′−Fe(1)−C(3)	85.85(10)
C(1)−Fe(1)−N(4)	176.20(10)	C(2)′−Fe(1)−N(4)	92.26(9)
C(3)−Fe(1)−N(4)	93.78(10)	C(1)−Fe(1)−N(6)	91.58(10)
C(2)′−Fe(1)−N(6)	176.11(10)	C(3)−Fe(1)−N(6)	90.27(10)
N(4)−Fe(1)−N(6)	88.16(9)	C(1)−Fe(1)−N(8)	89.16(10)
C(2)′−Fe(1)−N(8)	94.82(10)	C(3)−Fe(1)−N(8)	178.92(10)
N(4)−Fe(1)−N(8)	87.05(9)	N(6)−Fe(1)−N(8)	89.06(10)

[a] The estimated standard deviations are given in parentheses. [b] Symmetry code: (′) = 1 − *x*, 2 − *y*, 1 − *z*.

Table 5. Selected Bond Distances (Å) and Angles (deg) for 2b[a,b]

Ni(1)−N(1)	2.083(3)	Ni(1)−N(2)′	2.085(3)
Ni(1)−N(10)	2.137(3)	Ni(1)−N(11)	2.201(3)
Ni(1)−N(12)	2.148(3)	Ni(1)−N(13)	2.157(3)
Fe(1)−C(1)	1.940(3)	Fe(1)−C(2)	1.938(3)
Fe(1)−C(3)	1.951(3)	Fe(1)−N(4)	1.996(3)
Fe(1)−N(6)	1.979(3)	Fe(1)−N(8)	1.972(3)
N(1)−Ni(1)−N(2)′	86.28(10)	N(1)−Ni(1)−N(10)	175.32(10)
N(2)′−Ni(1)−N(10)	91.58(10)	N(1)−Ni(1)−N(11)	97.65(10)
N(2)′−Ni(1)−N(11)	81.55(10)	N(10)−Ni(1)−N(11)	77.90(10)
N(1)−Ni(1)−N(12)	84.60(10)	N(2)′−Ni(1)−N(12)	168.67(10)
N(10)−Ni(1)−N(12)	97.99(10)	N(11)−Ni(1)−N(12)	106.31(10)
N(1)−Ni(1)−N(13)	86.81(10)	N(2)′−Ni(1)−N(13)	93.78(10)
N(10)−Ni(1)−N(13)	97.49(10)	N(11)−Ni(1)−N(13)	173.27(10)
N(12)−Ni(1)−N(13)	79.03(10)	C(1)−Fe(1)−C(2)	88.79(12)
C(1)−Fe(1)−C(3)	90.15(13)	C(2)−Fe(1)−C(3)	89.33(13)
C(1)−Fe(1)−N(4)	177.86(12)	C(2)−Fe(1)−N(4)	90.34(12)
C(3)−Fe(1)−N(4)	91.81(13)	C(1)−Fe(1)−N(6)	92.82(12)
C(2)−Fe(1)−N(6)	178.39(12)	C(3)−Fe(1)−N(6)	90.59(12)
N(4)−Fe(1)−N(6)	88.05(11)	C(1)−Fe(1)−N(8)	89.85(12)
C(2)−Fe(1)−N(8)	91.49(12)	C(3)−Fe(1)−N(8)	179.17(12)
N(4)−Fe(1)−N(8)	88.21(11)	N(6)−Fe(1)−N(8)	88.59(11)

[a] The estimated standard deviations are given in parentheses. [b] Symmetry code: (′) = 1 − *x*, 2 − *y*, 1 − *z*.

Table 6. Selected Bond Distances (Å) and Angles (deg) for 3a[a,b]

Co(1)−N(1)	2.154(6)	Co(1)−N(2)	2.130(6)
Co(1)−N(10)	2.196(6)	Co(1)−N(11)	2.227(6)
Co(1)−N(12)	2.181(6)	Co(1)−N(13)	2.200(6)
Fe(1)−C(1)	1.949(7)	Fe(1)−C(2)′	1.947(7)
Fe(1)−C(3)	1.950(7)	Fe(1)−N(4)	1.999(6)
Fe(1)−N(6)	2.011(6)	Fe(1)−N(8)	1.973(6)
N(1)−Co(1)−N(2)	86.9(2)	N(1)−Co(1)−N(10)	174.3(2)
N(2)−Co(1)−N(10)	90.3(2)	N(1)−Co(1)−N(11)	97.6(2)
N(2)−Co(1)−N(11)	80.2(2)	N(10)−Co(1)−N(11)	77.1(2)
N(1)−Co(1)−N(12)	86.0(2)	N(2)−Co(1)−N(12)	172.2(2)
N(10)−Co(1)−N(12)	97.1(2)	N(11)−Co(1)−N(12)	103.9(2)
N(1)−Co(1)−N(13)	84.4(2)	N(2)−Co(1)−N(13)	98.6(2)
N(10)−Co(1)−N(13)	100.9(2)	N(11)−Co(1)−N(13)	177.6(2)
N(12)−Co(1)−N(13)	77.6(2)	C(1)−Fe(1)−C(2)′	88.1(3)
C(1)−Fe(1)−C(3)	89.6(3)	C(2)′−Fe(1)−C(3)	86.1(3)
C(1)−Fe(1)−N(4)	176.9(3)	C(2)′−Fe(1)−N(4)	91.7(3)
C(3)−Fe(1)−N(4)	93.5(3)	C(1)−Fe(1)−N(6)	91.7(3)
C(2)′−Fe(1)−N(6)	175.9(3)	C(3)−Fe(1)−N(6)	89.8(3)
N(4)−Fe(1)−N(6)	88.8(3)	C(1)−Fe(1)−N(8)	89.7(3)
C(2)′−Fe(1)−N(8)	95.2(3)	C(3)−Fe(1)−N(8)	178.5(3)
N(4)−Fe(1)−N(8)	87.3(3)	N(6)−Fe(1)−N(8)	88.9(3)

[a] The estimated standard deviations are given in parentheses. [b] Symmetry code: (′) = −*x*, 1 − *y*, −*z*.

interactions between the paramagnetic centers, which are linked by it. The reactions of cyanide-bearing $[Fe(L)(CN)_3]^-$ unit with first-row transition metals with four coordination positions blocked by two terminal ligands $[M(L')_2(S)_2]^{2+}$ (S = solvent) yield molecular squares with interesting and different (depending on M) magnetic properties. The $[Fe(L)(CN)_3]^-$ complex acts as a bis-monodentate ligand through two of its three cyanide groups, with the third one remaining free. This coordination

dx.doi.org/10.1021/ic200616p |*Inorg. Chem.* 2011, 50, 6250–6262

Table 7. Selected Bond Distances (Å) and Angles (deg) for 3b[a,b]

Fe(1)−N(4)	1.998(3)	Fe(1)−N(6)	1.975(3)
Fe(1)−N(8)	1.970(3)	Fe(1)−C(1)	1.933(4)
Fe(1)−C(2)	1.934(4)	Fe(1)−C(3)	1.944(4)
Co(1)−N(1)	2.127(3)	Co(1)−N(2)′	2.114(3)
Co(1)−N(10)	2.167(4)	Co(1)−N(11)	2.257(4)
Co(1)−N(12)	2.185(3)	Co(1)−N(13)	2.193(3)
N(4)−Fe(1)−N(6)	88.14(13)	N(4)−Fe(1)−N(8)	88.04(13)
N(6)−Fe(1)−N(8)	88.41(13)	N(4)−Fe(1)−C(1)	178.45(15)
N(6)−Fe(1)−C(1)	92.31(14)	N(8)−Fe(1)−C(1)	90.48(15)
N(4)−Fe(1)−C(2)	91.24(14)	N(6)−Fe(1)−C(2)	179.38(14)
N(8)−Fe(1)−C(2)	91.56(15)	C(1)−Fe(1)−C(2)	88.31(15)
N(4)−Fe(1)−C(3)	91.77(15)	N(6)−Fe(1)−C(3)	91.07(15)
N(8)−Fe(1)−C(3)	179.45(15)	C(1)−Fe(1)−C(3)	89.71(17)
C(2)−Fe(1)−C(3)	88.96(16)	N(1)−Co(1)−N(2)′	87.50(12)
N(1)−Co(1)−N(10)	174.70(14)	N(2)′−Co(1)−N(10)	91.78(13)
N(1)−Co(1)−N(11)	98.50(15)	N(2)′−Co(1)−N(11)	80.13(14)
N(10)−Co(1)−N(11)	76.21(15)	N(1)−Co(1)−N(12)	83.55(12)
N(2)′−Co(1)−N(12)	168.73(13)	N(10)−Co(1)−N(12)	97.75(13)
N(11)−Co(1)−N(12)	107.93(14)	N(1)−Co(1)−N(13)	86.82(13)
N(2)′−Co(1)−N(13)	95.55(12)	N(10)−Co(1)−N(13)	98.48(13)
N(11)−Co(1)−N(13)	172.94(15)	N(12)−Co(1)−N(13)	77.16(12)

[a] The estimated standard deviations are given in parentheses. [b] Symmetry code: (′) = $-x$, $1-y$, $-z$.

mode was previously observed in the related tetranuclear square of formula $[Fe^{III}\{HB(pz)_3\}(CN)_2(\mu\text{-}CN)Mn^{II}(bpy)_2]_2(ClO_4)_2\cdot 4CH_3CN$.[23a] The bonding mode is reflected in the IR spectra of the complexes. The presence of bridging and terminal cyanide ligands in these compounds is consistent with the observation of two stretching cyanide vibrations [ν(CN)] of medium (ca. 2000 cm^{-1}) and small (ca. 2050 cm^{-1}) intensities, respectively.

Descriptions of the Structures. *$[Fe^{III}\{B(pz)_4\}(CN)_2(\mu\text{-}CN)Mn^{II}(bpy)_2]_2(ClO_4)_2\cdot CH_3CN$ (**1**).* The crystal structure of **1** consists of discrete tetranuclear mixed metal units (Figure 1a), perchlorate anions, and free acetonitrile molecules (Figure S1, Supporting Information). Two $[Fe\{B(Pz)_4\}(CN)_3]^-$ units from each tetranuclear entity in **1** bridge two manganese(II) ions through two cyanide bridges to form [2 + 2]-type discrete molecular squares [N(1)′−Mn(1)−N(2) = 90.15(11)° and C(1)−Fe(1)−C(2) = 90.38(14)°]. The remaining coordination sites of each six-coordinated Mn(II) ion are occupied by two bidentate bpy molecules. The metal atom exhibits a distorted octahedral environment, MnN_6 (Figure 1b). An important bending occurs at one of the cyanide bridges, the value of the Mn(1)−N(2)−C(2) angle being 160.1(2)°, whereas the departure from linearity is much smaller at the other cyanide bridge [Mn(1)−N(1)′−C(1) = 173.3(2)°].

Each iron(III) ion in **1** shows a slightly distorted six-coordinated octahedral environment (Figure 1c), FeC_3N_3, formed by three imine-nitrogen atoms from the terminal $B(pz)_4^-$ ligand and three cyanide-carbon atoms. The Fe(III)−C(cyanide) distances are shorter than those of the Fe(III)−N(bpy). Selected bond distances and angles for **1** are listed in Table 3. The Fe−C−N angles depart slightly from linearity [175.0(2)−178.5(2)°], with the greater bending being observed for the Fe(1)−C(1)−N(1) angle.

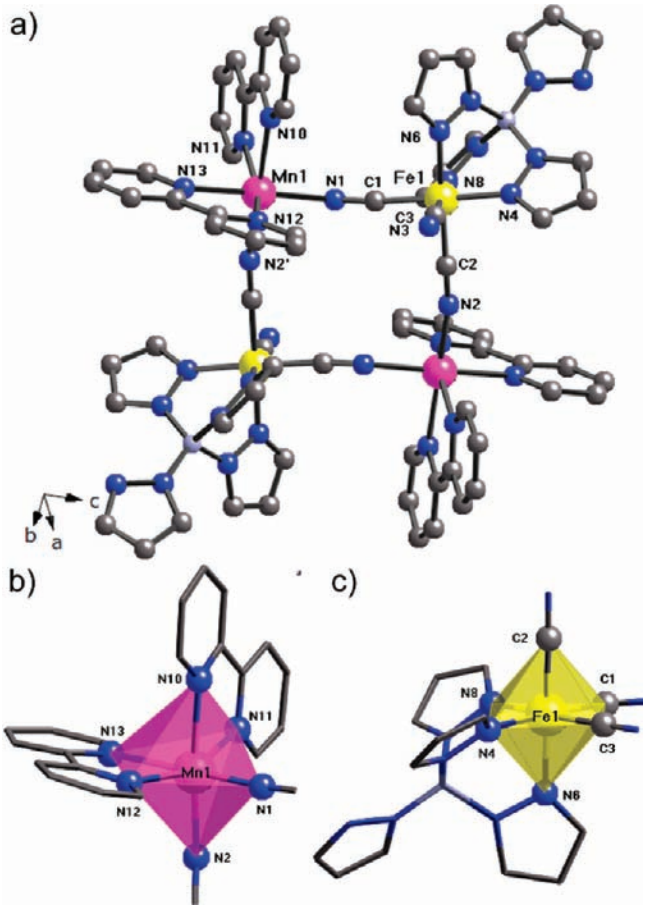

Figure 1. (a) Perspective view of the cationic tetranuclear $Fe^{III}_2Mn^{II}_2$ unit of **1** with the atom-numbering scheme for the metals' coordination environment. (b) and (c) Projection views of the surroundings for the manganese and iron atoms, respectively. The metal coordination spheres are depicted as polyhedra. Hydrogen atoms are omitted for clarity.

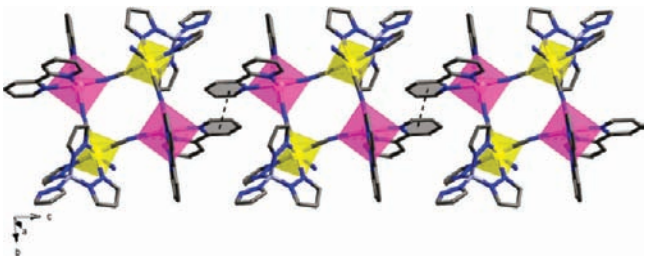

Figure 2. Perspective views of the $\pi-\pi$ stacking interactions between the bpy ligands (represented by dotted lines) in the [001] direction. The metal coordination spheres are depicted as polyhedra. Hydrogen atoms are omitted for clarity.

The values of the $Fe^{III}\cdots Mn^{II}$ distance through the cyanide bridges are 5.255(2) and 5.218(2) Å. The intramolecular Fe(1)···Mn(1)···Fe(1)′ and Mn(1)···Fe(1)···Mn(1)′ angles are 88.831(9) and 91.169(10)°. These values are similar to those reported in the related tetranuclear square compound $[Fe^{III}\{HB(pz)_3\}(CN)_2(\mu\text{-}CN)Mn^{II}(bpy)_2]_2(ClO_4)_2\cdot 4CH_3CN$.[23a]

Weak intermolecular $\pi-\pi$ interactions between adjacent bpy molecules coordinated to the Mn(II) ions lead to a supramolecular chainlike structure along the [001] direction (Figure 2)

dx.doi.org/10.1021/ic200616p |*Inorg. Chem.* 2011, 50, 6250–6262

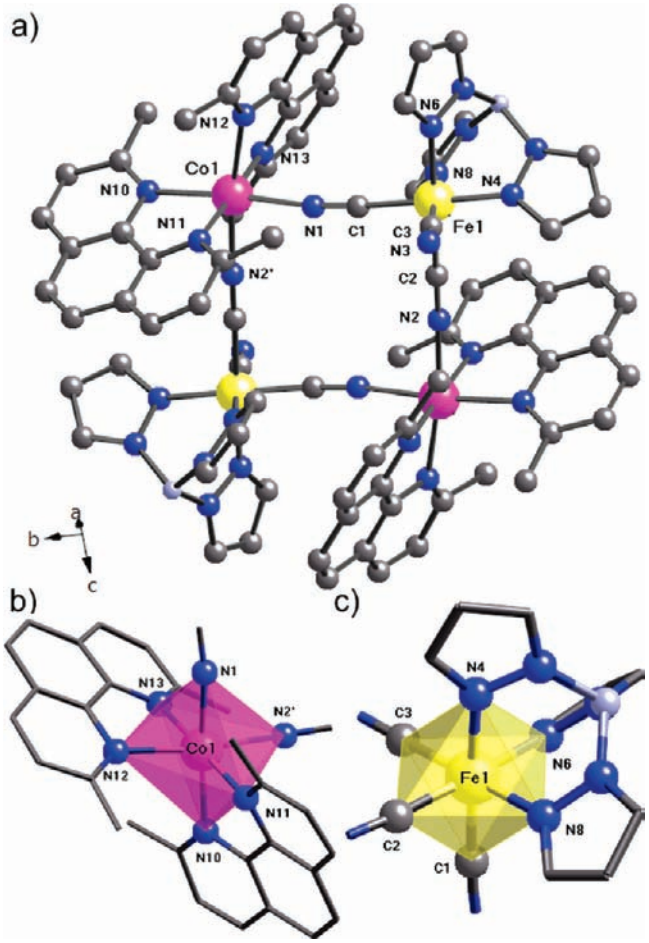

Figure 3. (a) Perspective view of the cationic tetranuclear $Fe^{III}_2Co^{II}_2$ unit of **2b** with the atom-numbering scheme for the metal coordination environments. (b) and (c) Projection views of the metal coordination environment for the cobalt and iron atoms, respectively. The metal coordination spheres are depicted as polyhedra. Hydrogen atoms are omitted for clarity.

with centroid−centroid distances between the bpy planes of 3.642(2) Å.

$[Fe^{III}\{HB(pz)_3\}(CN)_2(\mu\text{-}CN)Ni^{II}(dmphen)_2]_2(ClO_4)_2\cdot 2CH_3OH$ (***2a***) *and* *$[Fe^{III}\{HB(pz)_3\}(CN)_2(\mu\text{-}CN)Co^{II}(dmphen)_2]_2(ClO_4)_2\cdot 2CH_3OH$* (***3a***). Compounds **2a** and **3a** are isostructural and are described together. They consist of discrete tetranuclear mixed metal units (Figure 3), perchlorate anions, and crystallization methanol molecules (Figure S2, Supporting Information). The overall structure of the cationic tetranuclear complexes can be described as [2 + 2]-type tetranuclear squares formed by two low-spin Fe^{III} ions and two high-spin Ni^{II} (**2a**) or Co^{II} (**3a**) ions linked through two cyanide groups of the *fac*-$[Fe^{III}\{HB(pz)_3\}(CN)_3]^-$ complex (Figure 3a). The iron(III) precursor coordinates in a bis-monodentate manner through two of its three cyanide groups toward the $[M(dmphen)_2]^{2+}$ [M = Ni (**2a**) and Co(**3a**)] cationic units [N(1)−Ni(1)−N(2) = 86.58(10)° and C(1)−Fe(1)−C(2)′ = 88.26(11)° for **2a** and N(1)−Co(1)−N(2) = 86.88(21)° and C(1)−Fe(1)−C(2)′ = 88.26(11)° for **3a**], with the third cyanide group remaining terminal. The separation between adjacent metal atoms within the tetranuclear units through the cyanide bridges are 5.170(6) and 5.166(8) Å in **2a** and 5.229(1) and 5.212(1) Å in **3a**, respectively. The intramolecular Fe(1)···M(1)···Fe(1)′ and M(1)···Fe(1)···M(1)′ angles are 88.27(4) and 91.73(4)° in **2a** and 88.60(2) and 91.40(2)° in **3a**, respectively.

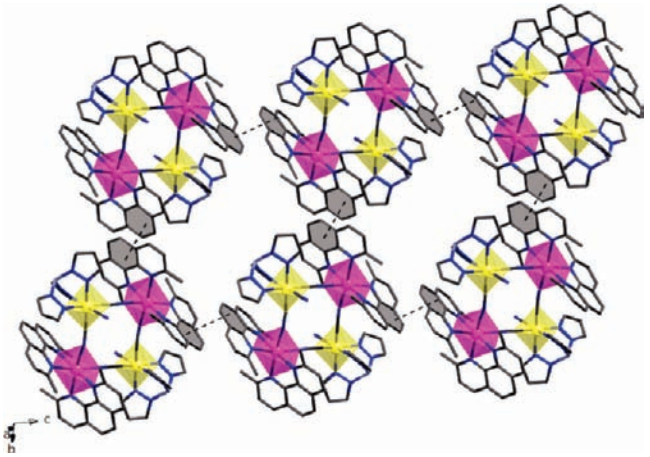

Figure 4. Perspective views of the $\pi-\pi$ stacking interactions between the dmphen ligands (represented by dotted lines) forming a 2D motif. The metal coordination spheres are depicted as polyhedra. Hydrogen atoms are omitted for clarity.

The two iron(III) atoms of **2a** and **3a** show a slightly distorted six-coordinated octahedral environment, FeC_3N_3 (Figure 3c), formed by three pyrazolyl-nitrogen atoms from the capping $HB(Pz)_3^-$ ligand and three cyanide-carbon atoms from the terminal and bridging cyanide groups. The Fe(III)−C(cyanide) and Fe(III)−N(dmphen) distances (Tables 4 and 5) are similar to those found in **1** and in the related tetranuclear compound $[Fe^{III}\{HB(pz)_3\}(CN)_2(\mu\text{-}CN)M^{II}(DMF)_2]_2(OTf)_2\cdot 2DMF$.[17a] The Fe−C−N angles are not far away from linearity [175.8(2)−176.9(2)° for **2a** and 176.3(6)−176.9(6)° for **3a**].

On the other hand, the two Ni(II) atoms of **2a** and the two Co(II) atoms of **3a** exhibit a distorted octahedral environment, MN_6, which is formed by four imine-nitrogen atoms from the terminal dmphen ligands and two cyanide-nitrogen atoms from the two bridging cyanide groups. The M(II)−N(cyanide) bond distances are all shorter than the M(II)−N(dmphen) bond lengths (Tables 4 and 5). This situation contrasts with that observed in the related tetranuclear compounds $[Fe^{III}\{HB(pz)_3\}(CN)_2(\mu\text{-}CN)M^{II}(DMF)_2]_2(OTf)_2\cdot 2DMF$ (M = Ni and Co),[17a] where the octahedral environments around Ni^{II} and Co^{II} ions are less distorted. An important departure from linearity at the M−N−C angles occurs for **2a** and **3a**, where the values of the M(1)−N(1)−C(1) and M(1)−N(2)−C(2) angles are 169.5(2) and 168.6(2)° for **2a** (M = Ni) and 169.3(6) and 170.3(5)° for **2b** (M = Co), respectively. Selected bond distances and angles for **2a** and **3a** are listed in Tables 4 and 5 respectively.

There is a perfect alignment of tetranuclear molecules along the [100] direction in the crystal lattice (Figure 4). Weak intermolecular $\pi-\pi$ type interactions between several adjacent dmphen molecules coordinated to M(II) ions occur in the *ac* plane, resulting in a supramolecular 2D-like structure with centroid−centroid distances between dmphen planes of 3.668(2) and 3.550(2) Å for **2a** and 3.660(5) and 3.571(5) Å for **3a** (Figure 4). The shortest intermolecular Fe(1)···Fe(1)′, M(1)···M(1)′, and Fe(1)···M(1)′ distances are 8.840(2), 10.143(2), and 8.943(2) Å for **2a** and 8.955(1), 10.206(2), and 8.954(2) Å for **3a**.

dx.doi.org/10.1021/ic200616p |*Inorg. Chem.* 2011, 50, 6250–6262

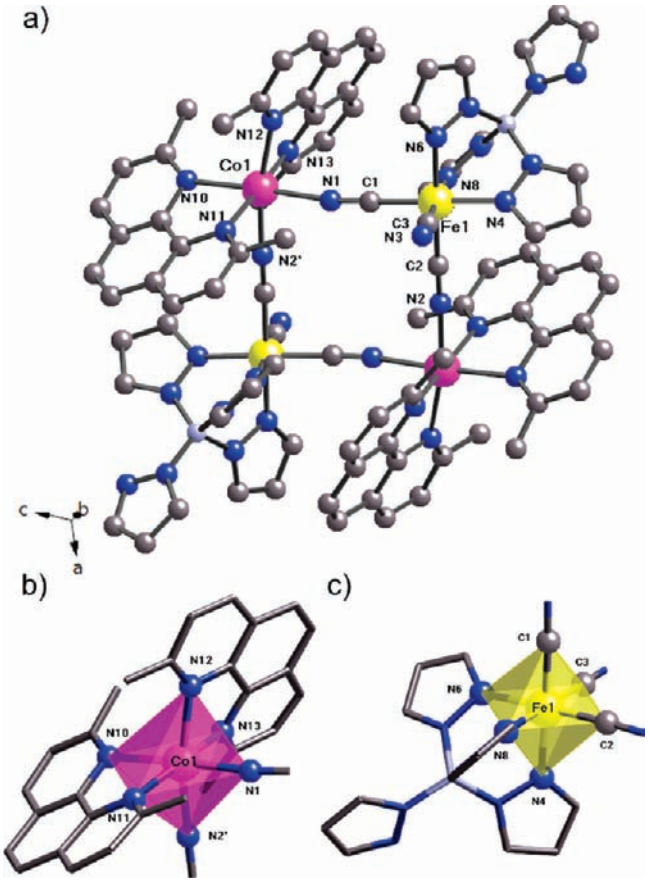

Figure 5. (a) Perspective view of the cationic tetranuclear $Fe^{III}_2Co^{II}_2$ unit of **3b** with the atom-numbering scheme for the metal coordination environments. (b) and (c) Projection views of the metal coordination environment for the cobalt and iron atoms, respectively. The metal coordination spheres are depicted as polyhedra. Hydrogen atoms are omitted for clarity.

$[Fe^{III}\{B(pz)_4\}(CN)_2(\mu\text{-}CN)Ni^{II}(dmphen)_2]_2(ClO_4)_2\cdot 2CH_3OH$ (***2b***) *and* $[Fe^{III}\{B(pz)_4\}(CN)_2(\mu\text{-}CN)Co^{II}(dmphen)_2]_2(ClO_4)_2\cdot 2CH_3OH$ (***3b***). Compounds **2b** and **3b** are isostructural, and they are described together. The crystal structure of **2b** and **3b** is similar to that observed for **2a** and **3a**, and it consists of discrete tetranuclear mixed metal complexes (Figure 5), perchlorate anions, and crystallization methanol molecules (Figure S3, Supporting Information). Two *fac*-$[Fe^{III}\{B(pz)_4\}(CN)_3]^-$ units in **2b** and **3b** act as bridges in a bis-monodentate way toward two M(II) ions [M = Ni (**2b**) and Co (**3b**)] through two cyanide ligands to form the same [2 + 2]-type tetranuclear squares with two low-spin Fe^{III} ions and two high-spin Ni^{II} (**2b**) or Co^{II} (**3b**) ions at the corners of the square (Figure 5a). The coordination mode of the $[Fe^{III}\{B(pz)_4\}(CN)_3]^-$ species is bis-monodentate toward the $[M(dmphen)_2]^{2+}$ cationic units [M = Ni (**2b**) and Co (**3b**)]. The values of the N(1)−M(1)−N(2)′ and C(1)−Fe(1)−C(2) angles are 86.28(10) and 88.79(12)° for **2b** and 87.50(12) and 88.31(15)° for **3b**. The separations between neighboring metal atoms within the tetranuclear units through the cyanide bridges are 5.150(6) and 5.168(5) Å in **2b** and 5.191(1) and 5.199(1) Å in **3b**. The intramolecular Fe(1)···M(1)···Fe(1)′ and M(1)···Fe(1)···M(1)′ angles are 87.68(3) and 92.32(3)° in **2b** and 88.54(1) and 91.46(1)° in **3b**, respectively. Selected bond distances and angles for **2b** and **3b** are listed in Tables 6 and 7, respectively.

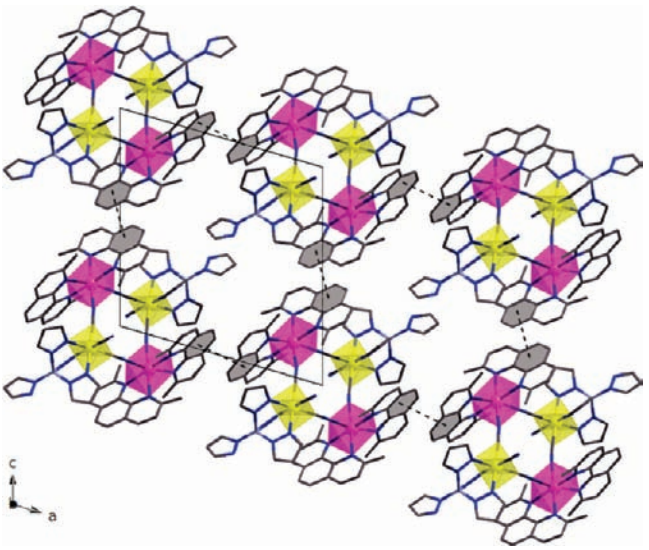

Figure 6. Perspective views of the $\pi-\pi$ stacking interactions between the dmphen ligands (represented by dotted lines) in the *ac* plane. The metal coordination spheres are depicted as polyhedra. Hydrogen atoms are omitted for clarity.

The two Fe(III) atoms of **2b** and **3b** show a slightly distorted six-coordinated octahedral environment, FeC_3N_3 (Figure 5c), which is formed by three imine-nitrogen atoms from the capping $B(pz)_4^-$ ligand and three cyanide-carbon atoms from one terminal and two bridging cyanide groups. The Fe(III)−C(cyanide) and the Fe(III)−N(dmphen) distances are similar to those found in the former complexes (Tables 6 and 7). The Fe−C−N angles in both compounds are close to linearity [176.3(3)−176.5(3)° for **2b** and 177.0(3)−177.2(3)° for **3b**].

The two Ni(II) atoms of **2b** and the two Co(II) atoms of **3b** exhibit a distorted octahedral environment, MN_6, which is formed by four imine-nitrogen atoms from the terminal dmphen ligands and two cyanide-nitrogen atoms from the two bridging cyanide groups. The M(II)−N(cyanide) distances are all shorter than the M(II)−N(dmphen) distances (Tables 6 and 7). This severe distortion is higher than that observed for the related tetranuclear compounds $[Fe^{III}\{HB(pz)_3\}(CN)_2(\mu\text{-}CN)M^{II}(DMF)_2]_2(OTf)_2\cdot 2DMF$ (M = Ni, Co).[17a] In a similar manner to that seen in **2a** and **3a**, significant departures from linearity at the M−N−C angle for **2b** and **3b** occur, where the values of the M(1)−N(1)−C(1) and M(1)−N(2)′−C(2) angles are 170.3(3) and 171.6(3)° for **2b** (M = Ni) and 170.5(3) and 172.3(3)° for **2b** (M = Co), respectively.

There is a perfect alignment of tetranuclear molecules along the [010] direction in the crystal lattice (Figure S3, Supporting Information). Weak intermolecular $\pi-\pi$ type interactions between several adjacent dmphen molecules coordinated to M(II) ions in the *ac* plane result in a supramolecular 2D-like structure with values of the centroid−centroid distance between the two dmphen planes of 3.802(2) and 3.568(2) Å for **2b** and 3.801(5) and 3.636(5) Å for **3b** (Figure 6). The shortest intermolecular Fe(1)···Fe(1)′, M(1)···M(1)′, and Fe(1)···M(1)′ distances are 9.419(2), 10.206(2), and 8.250(2) Å in **2b** and 9.447(1), 10.325(1), and 8.206(1) Å in **3b**, respectively.

Magnetic Properties of 1−3b. The $\chi_M T$ versus T plots of **1** (χ_M is the molar magnetic susceptibility per $Fe^{III}_2Mn^{II}_2$ unit) is

dx.doi.org/10.1021/ic200616p |*Inorg. Chem.* 2011, 50, 6250–6262

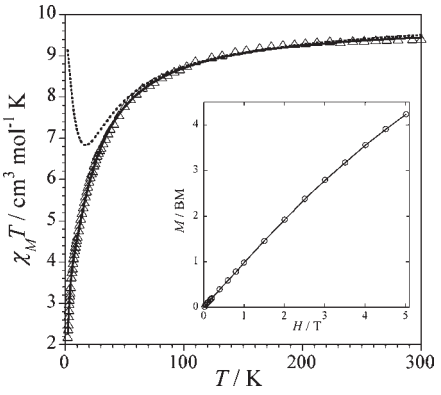

Figure 7. Temperature dependence of $\chi_M T$ for **1** (△) in an applied magnetic field of 1 T ($T \geq 30$ K) and 100 G ($T < 30$ K). Lines are the best-fit curves taking into account the intermolecular interactions θ (solid) or not (dotted). The inset shows the field dependence of M of **1** (○) at 2.0 K. The solid line is a guide for the eye.

consistent with antiferromagnetically coupled $Fe^{III}_2Mn^{II}_2$ tetranuclear squares (Figure 7). At room temperature, $\chi_M T$ is equal to 9.42 cm^3 K mol^{-1}, a value which is slightly smaller than the sum of two magnetically isolated low-spin Fe^{III} ions ($\chi_M T$ = 0.50 cm^3 K mol^{-1} per iron atom with g_{Fe} = 2.3) and two high-spin Mn^{II} ions ($\chi_M T$ = 4.37 cm^3 K mol^{-1} per manganese atom with g_{Mn} = 2.0). Upon cooling, $\chi_M T$ continuously decreases first slowly from 9.42 to 8.78 cm^3 K mol^{-1} and then more abruptly below ca. 100 K, reaching a minimum value of 2.19 cm^3 K mol^{-1} at 2.0 K. This magnetic behavior is similar to that reported for the related tetranuclear compounds $[Fe^{III}\{HB(pz)_3\}(CN)_2(\mu\text{-}CN)Mn^{II}(DMF)_2]_2[OTf]_2\cdot 2DMF$[17a] and $[Fe^{III}\{HB(pz)_3\}(CN)_3]_2[Mn(bpy)_4]_2[ClO_4]_2$.[23a] The value of $\chi_M T$ at 2.0 K is below that expected for an S = 4 ground spin state.

The M versus H plot for **1** at 2.0 K is shown in the inset of Figure 7. M is the magnetization per $Fe^{III}_2Mn^{II}_2$ unit. The magnetization at 5.0 T (M = 4.22 μ_B) is well below that expected for an S = 4 ground state, but it has not reached the saturation.

The analysis of the magnetic susceptibility data of compound **1** was carried out by full-matrix diagonalization[33] of the appropriate isotropic spin Hamiltonian for a tetranuclear $Fe^{III}_2Mn^{II}_2$ square model [eq 1 with M = Mn; $\mathbf{S}_{M1} = \mathbf{S}_{M2} = 5/2$ and $\mathbf{S}_{Fe1} = \mathbf{S}_{Fe2} = 1/2$] (see Chart 1):

$$\hat{H} = -J_1[\hat{S}_{Fe1}\cdot\hat{S}_{M1} + \hat{S}_{Fe2}\cdot\hat{S}_{M2}] - J_2[\hat{S}_{Fe1}\cdot\hat{S}_{M2} + \hat{S}_{Fe2}\cdot\hat{S}_{M1}] + g_{Fe}(\hat{S}_{Fe1} + \hat{S}_{Fe2})H\beta + g_M(\hat{S}_{M1} + \hat{S}_{M2})H\beta \quad (1)$$

where J_1 and J_2 are the two intramolecular magnetic coupling parameters, g_{Mn} and g_{Fe} are the Landé factors of the Mn^{II} and Fe^{III} ions, β is the Bohr magneton, and H is the applied magnetic field. The intermolecular interactions are taken into account by using a Weiss constant (θ) in the form of $T - \theta$ in the expression giving the susceptibility. Although **1**−**3b** can be considered as squares from a structural point of view, we have to use two independent J parameters (J_1 and J_2) due to the existence of two significantly different values for the M−N−C angles and Fe−M distances (see Descriptions of the Structures). In fact, it is not possible to obtain a good fit of the experimental data by using only one J parameter.

The least-squares fit of the experimental data gives g_{Fe} = 2.32, g_{Mn} = 1.99, J_1 = −2.70 cm^{-1}, J_2 = −6.20 cm^{-1}, and θ = −4.70 K [where θ is the Weiss factor defined as $\theta = zjS(S+1)/3k$ with S = 4 and zj = −0.49 cm^{-1}] (Table 8). The fitted plot (solid line in Figure 7) closely follows the experimental data in the whole temperature range 300−2 K. The negative J values reflect the antiferromagnetic coupling due to the overlap of the Fe and Mn t_{2g} orbitals (local symmetry), whereas the antiferromagnetic intermolecular interactions are reflected in the negative value of θ as can be expected from the intermolecular π−π bipyridine orbital overlap between tetranuclear cations in the [001] direction (closest bypiridine ring contact of 3.34 Å shown in Scheme 1a).

Table 8. Best Fit Magnetic Data for 1−3b

	J_1[a] (cm^{-1})	J_2[a] (cm^{-1})	g_{Fe}[b]	g_M[b]	zj[c] (cm^{-1})	θ[c] (cm^{-1})
1	−6.2	−2.7	2.32	1.99	−0.49	−4.7
2a	21.4	19.4	2.30	2.21	0.09	0.5
2b	17.0	12.5	2.39	2.20	0.61	3.5
3a	5.4	11.1	2.30	–	−0.03	−0.1
3b	8.1	11.0	2.33	–	0	0

[a] J_1 and J_2 are the exchange magnetic coupling parameters through the crystallographically independent heterobimetallic units: Fe(1)−C(1)−N(1)−M(1) and Fe(1)−C(2)−N(2)−M(1), respectively. [b] Landé factors [M = Mn (**1**), Ni (**2a**, **2b**), and Co (**3a**, **3b**)]. [c] Intermolecular exchange magnetic coupling.

Scheme 1. π−π Stacking Interactions in 1−3b Showing the Antiferromagnetic Pathway (a) for 1, and the Ferromagnetic (b) and Antiferromagnetic (c) Contributions in 2a−3b[a]

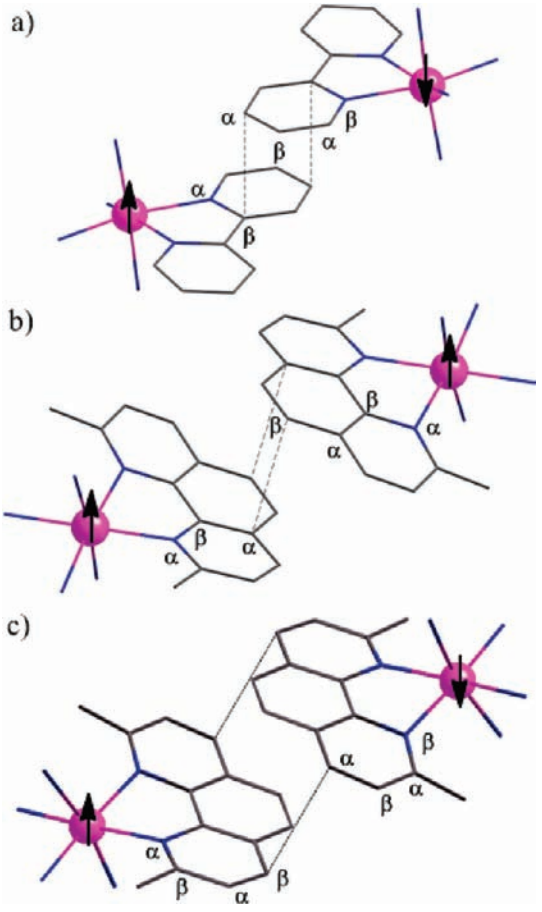

[a] α and β represent the alternative spin densities on the ligand atoms (up and down, respectively).

dx.doi.org/10.1021/ic200616p |Inorg. Chem. 2011, 50, 6250–6262

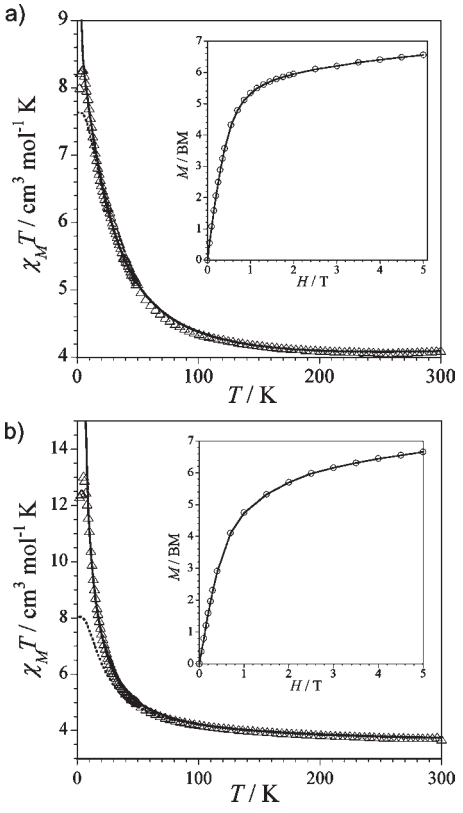

Figure 8. Temperature dependence of $\chi_M T$ (△) for **2a** (a) and **2b** (b) in an applied magnetic field of 1 T ($T \geq 30$ K) and 100 G ($T < 30$ K). Lines are the best-fit curves taking into account the intermolecular interactions θ (solid) or not (dotted). The insets show the field dependence of M (○) of **2a** (a) and **2b** (b) at 2.0 K. The solid lines are guides for the eye.

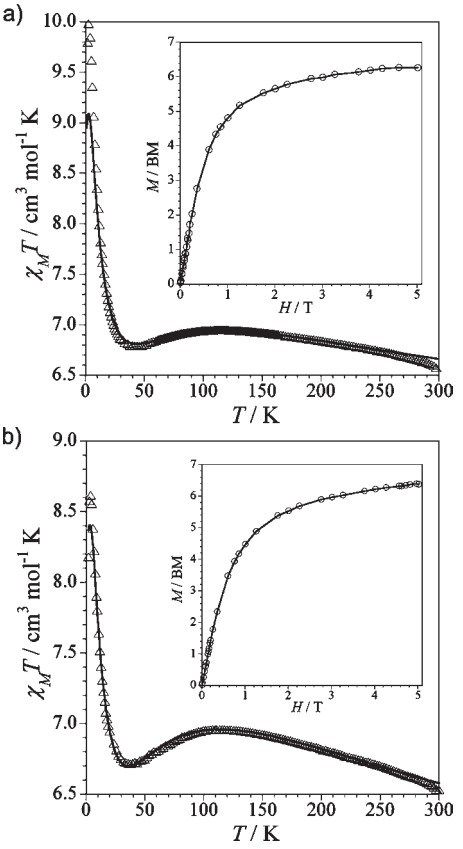

Figure 9. Temperature dependence of $\chi_M T$ (△) for **3a** (a) and **3b** (b) in an applied magnetic field of 1 T ($T \geq 30$ K) and 100 G ($T < 30$ K). Solid lines are the best-fit curves. The insets show the field dependence of M (○) of **3a** (a) and **3b** (b) at 2.0 K, with the solid lines being guides for the eye.

In Scheme 1 are shown the alternative spin densities [up (α) and down (β)] on the ligand atoms following a spin polarization mechanism. The J values obtained are similar to those determined for the related compound of formula $[Fe^{III}\{HB(pz)_3\}(CN)_3]_2$-$[Mn(bpy)_4]_2[ClO_4]_2$[23a] ($J_1 = -1.52$ cm^{-1}, $J_2 = -4.58$ cm^{-1}).

The $\chi_M T$ versus T plots (χ_M is the molar magnetic susceptibility per $Fe^{III}_2Ni^{II}_2$ unit) for **2a** and **2b** show qualitatively a similar magnetic behavior, consistent with ferromagnetically coupled $Fe^{III}_2Ni^{II}_2$ tetranuclear squares (Figure 8). At room temperature, the values of $\chi_M T$ are 4.09 and 3.72 cm^3 K mol^{-1} for **2a** and **2b**, respectively. These values are larger than those expected for the sum of two magnetically isolated low-spin Fe^{III} ions ($\chi_M T = 0.50$ cm^3 K mol^{-1} per iron atom with $g_{Fe} = 2.3$) and two high-spin Ni^{II} ions ($\chi_M T = 1.10$ cm^3 K mol^{-1} per nickel atom with $g_{Ni} = 2.1$). Upon cooling, $\chi_M T$ increases smoothly until ca. 50 K, in line with a ferromagnetic coupling between the Ni(II) and Fe(III) atoms through the cyanide bridges. At $T <$ 50 K, $\chi_M T$ sharply increases to reach maxima of ca. 8.26 and 13.03 cm^3 K mol^{-1} at 4.5 and 5.0 K for **2a** and **2b**, respectively. Then, it further decreases with T because of zero-field splitting and/or intermolecular interactions to reach values of 7.98 (**2a**) and 12.26 (**2b**) cm^3 K mol^{-1} at 2.0 K. These features are consistent with a ferromagnetic intrasquare interaction leading to an $S = 3$ ground spin state.

The M versus H plots for **2a** and **2b** at 2.0 K are shown in the insets of Figure 8. M is the magnetization per $Fe^{III}_2Ni^{II}_2$ unit. The magnetization values at 5.0 T ($M_s = 6.55$ and 6.60 μ_B for **2a** and **2b**, respectively) are consistent with the predicted one for an $S = 3$ ground spin state.

The analysis of the magnetic susceptibility data of compounds **2a** and **2b** were carried out by full-matrix diagonalization[33] of the isotropic spin Hamiltonian for a tetranuclear $Fe^{III}_2Ni^{II}_2$ square model [eq 1 with M = Ni; $S_{M1} = S_{M2} = 1$ and $S_{Fe1} = S_{Fe2} = 1/2$].

The intermolecular interactions were taken into account by using a Weiss constant (θ) in the form of $T - \theta$.

The least-squares fit of the experimental data of **2a** and **2b** are given in Table 8. The calculated plots (solid lines in Figure 8) closely follow the experimental data in the 300−8 and 300−6 K temperature ranges, respectively. The ferromagnetic intermolecular interactions between adjacent tetranuclear cations are reflected in the values of θ (+0.5 and +3.5 cm^{-1} for **2a** and **2b**, respectively; see Table 8). The positive θ values support the presence in both cases of an intermolecular ferromagnetic interaction [closest dmphen ring contacts of 3.42 and 3.40 Å for **2a** and **2b**, respectively (Scheme 1b)]. The lower value of θ obtained for **2b** must be related to a weaker ferromagnetic $\pi-\pi$ interaction through the aromatic dmphen rings compared to that in **2a** [closest dmphen ring contacts of 3.37 and 3.40 Å for **2a** and **2b** (Scheme 1c)].

The $\chi_M T$ versus T plots (χ_M is the molar magnetic susceptibility per $Fe^{III}_2Co^{II}_2$ unit) of **3a** and **3b** show qualitatively a similar magnetic behavior (Figure 9). At room temperature, the

dx.doi.org/10.1021/ic200616p |*Inorg. Chem.* 2011, 50, 6250–6262

values of $\chi_M T$ are 6.57 and 6.53 cm^3 K mol^{-1} for **3a** and **3b**, respectively. They compare well with that expected for the sum of two magnetically isolated low-spin Fe^{III} ions ($\chi_M T$ = 0.50 cm^3 K mol^{-1} per iron atom with g_{Fe} = 2.3) and two octahedral high-spin Co^{II} ions (S_{Co} = 3/2) with an orbitally degenerate $^4T_{1g}$ single-ion ground state with significant orbital contributions ($\chi_M T$ = 2.5−3.0 cm^3 K mol^{-1} per cobalt(II) ion).[34] On cooling, $\chi_M T$ increases first to attain broad maxima at 110 (**3a**) and 115 K (**3b**) and further decreases due to the spin−orbit coupling of the Co^{II} ions reaching minima at 44 (**3a**) and 38 K (**3b**) (insets of Figure 9). After the minima, $\chi_M T$ sharply increases to reach maxima of 10.0 and 8.61 cm^3 K mol^{-1} at 2.50 (**3a**) and 3.72 K (**3b**). Finally, the decrease of the $\chi_M T$ product at low temperature is probably due to intermolecular interactions and/or the magnetic anisotropy of cobalt(II) ions.

The magnetization M vs H plots for **3a** and **3b** at 2.0 K are shown in the insets of Figure 9. M is the magnetization per $Fe^{III}_2Co^{II}_2$ unit. The magnetization values at 5.0 T (M_s = 6.26 and 6.40 μ_B for **3a** and **3b**, respectively) are consistent with the predicted value (M_s = 6.50 μ_B) for an S = 2 state resulting from the ferromagnetic coupling between two low-spin Fe^{III} (S_{Fe} =1/2 with g = 2.3) and two high-spin Co^{II} ions (S_{eff} = 1/2 with g = 4.2).[34]

In order to analyze the magnetic susceptibility data of compounds **3a** and **3b**, we have used the isotropic spin Hamiltonian mentioned above [eq 1 with M = Co; $\mathbf{S}_{M1} = \mathbf{S}_{M2}$ = 3/2], in which we have included three other terms [eqs 2−4]:

$$\hat{H}_{so} = \sum_{i=1}^{2} A\kappa\lambda[\hat{L}_{Co1}\cdot\hat{S}_{Co1} + \hat{L}_{Co2}\cdot\hat{S}_{Co2}] \quad (2)$$

$$\hat{H}_{ax} = \sum_{i=1}^{2} \Delta\left[\hat{L}^2_{zCo1} + \hat{L}^2_{zCo2} - \frac{4}{3}\right] \quad (3)$$

$$\hat{H}_{orb} = \sum_{i=1}^{2} -A\kappa[\hat{L}_{Co1} + \hat{L}_{Co2}]\beta H \quad (4)$$

where λ is the spin−orbit parameter and κ and A are orbital reduction factors associated with the covalent character of the metal−ligand bonds and with the interaction between the $^4T_{1g}$ ground state ($^4T_{1g}$[F]) and the excited $^4T_{1g}$ state from the P term ($^4T_{1g}$[P]).

The first term [eq 2] accounts for the spin−orbit coupling of the six-coordinated high-spin Co^{II} cations. The second one [eq 3] considers the axial distortion of the orbital triplet ground state $^4T_{1g}$, yielding an energy gap Δ between the $^4A_{2g}$ and ^4E_g states resulting from the splitting of this orbital triplet. Finally, the last term [eq 4] takes into account the orbital magnetic contribution of each Co^{II} ion. In all these three terms, we have used L = 1 corresponding to the isomorphism between the orbital triplet T_{1g} and a P term ($\|T_1\| = -A\|P\|$).

No analytical expression of the magnetic susceptibility can be derived through this Hamiltonian. The parameters J_1, J_2, A, k, λ, and Δ were determined instead through a numerical matrix diagonalization method.[33]

The parameters obtained from the best fit of the described model to the experimental data of **3a** and **3b** are the following: Ak = 1.20, λ = −122 cm^{-1}, Δ = −671 cm^{-1}, J_1 = +5.4 cm^{-1}, and J_2 = +11.1 cm^{-1} for **3a** and Ak = 1.10, λ = −101 cm^{-1}, Δ = −279 cm^{-1}, J_1 = +8.1 cm^{-1}, and J_2 = +11.0 cm^{-1} for **3b** (Table 8). These values are similar to those observed in other similar six-coordinated cobalt(II) complexes.[34] As done previously, the intermolecular interactions were taken into account by using a Weiss constant (θ) in the form of $T - \theta$. The fit of the experimental data gave values for θ of −0.1 (**3a**) and 0 (**3b**) cm^{-1}.

Most of these parameters are similar for **3a** and **3b**, but a large difference exists in the Δ parameter. We suggest that this feature is related to the tetragonal distortion and the spin−orbit coupling associated with the cobalt(II) ion[34] since large differences are found in the N−Co−N angles between the two complexes (see Descriptions of the Structures). For the fitted θ values, we suggest that they are not unambiguous due to the large number of parameters used in the fit of the magnetic data. Indeed, by looking at the crystal packing (Scheme 1), ferromagnetic intercluster interactions could be expected in a similar manner to **2**.

The magnetic behavior observed in complexes **1**-**3b** is somewhat similar to that found in related cyanometalate one-dimensional compounds and clusters. Thus, the interaction found through the cyanide bridges in heterometallic Fe^{III}−CN−M^{II} units is usually found to be antiferromagnetic when M = Mn[17a,18b,18c,23a] and ferromagnetic when M = Ni[17a,18d] and Co.[14a−c,17a,18a−18c] The causes of the different magnetic behaviors observed in compounds **1**−**3b** have been interpreted by carrying out theoretical calculations (below).

A final observation is that no out-of-phase *ac* signals usually found in SMMs have been observed in **1**−**3b** in contrast to the family $[Fe^{III}\{HB(pz)_3\}(CN)_2(\mu\text{-}CN)M^{II}(DMF)_2]_2[OTf]_2\cdot 2DMF$ (M = Ni, Co) where the frequency dependence of χ'' at very low temperatures was observed.[17a]

Theoretical Calculations. We performed electronic structure calculations based on density functional theory (DFT) for compounds **1**, **2b**, and **3b** following the method described under Computational Details. The results are summarized in Table 9.

An inspection of Table 9 shows that the J values obtained from DFT calculations for **1**, **2b**, and **3b** are in good agreement with those found from the fit of the magnetic data and also with those reported in a previous theoretical study on similar tetranuclear complexes.[35] These DFT calculations allow correlation of the values of the magnetic coupling with the geometric parameters of the exchange pathways. They provide also a simple orbital explanation. The iron(III) ion shows a low-spin configuration (t_{2g}^5) due to the strong ligand field mainly provided by the cyanide groups coordinated to the metal center through the carbon atom,[18c,36a−36e] whereas the six-coordinated manganese(II) (**1**), nickel(II) (**2b**), and cobalt(II) (**3b**) show high-spin electronic configurations [$t_{2g}^3e_g^2$ (**1**), $t_{2g}^6e_g^2$ (**2b**), and $t_{2g}^5e_g^2$ (**3b**)]. The unpaired electron of the low-spin iron(III) (in the singly occupied molecular orbital or magnetic orbital) in **1**, **2b**, and **3b** is defined by a mixture of the d_{xz} and d_{yz} type orbitals, in equal amounts. This composition is determined by the strength and the symmetry of the ligand field. The t_{2g} iron(III) orbital is delocalized on the π orbitals of the cyanide bridge and provides a π exchange pathway.[30,36a,36c,36e] The spin density map of **1** nicely illustrates this analysis (Figure 10).[30]

In the $Fe^{III}_2Ni^{II}_2$ compound (**1**),[18c,30,36a,36c,36d] the nickel(II) magnetic orbitals are $d_{x^2-y^2}$ and d_{z^2}. Only the last one interacts with the iron(III) magnetic orbital. When the Fe−C−N−M unit is linear, the strict orthogonality between the interacting magnetic orbitals causes the observed ferromagnetic coupling (Table 9). When the M t_{2g} magnetic orbitals become involved [i.e., in $Fe^{III}_2M^{II}_2$, M = Mn], antiferromagnetic terms arising

dx.doi.org/10.1021/ic200616p |*Inorg. Chem.* 2011, 50, 6250–6262

Table 9. Relevant Structural Parameters[a] and Values of the Exchange Coupling (J_i) in 1, 2b, and 3b (Computed by DFT and Fitted from Experiments)

compound	d_{Fe-M} (Å)	d_{Fe-C} (Å)	d_{M-N} (Å)	Fe−C−N (deg)	Mn−N−C (deg)	J_{theo} (cm^{-1})	J_{exp} (cm^{-1})
1	5.255/5.218	1.931/1.942	2.192/2.196	175.0/178.5	173.3/160.1	−4.6/−10.3	−2.7/−6.2
2b	5.150/5.168	1.939/1.937	2.083/2.085	176.3/176.5	170.3/171.6	16.5/12.6	17.0/12.5
3b	5.191/5.193	1.933/1.934	2.127/2.114	177.0/177.2	170.5/172.3	7.8/10.8	8.1/11.0

[a] For the two crystallographically independent heterobimetallic units: Fe(1)−C(1)−N(1)−M(1)/Fe(1)−C(2)−N(2)−M(1).

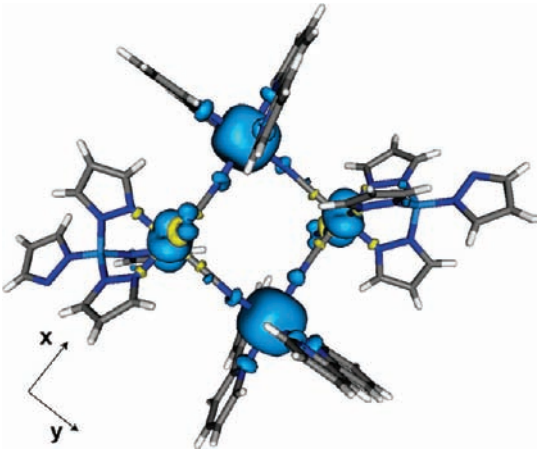

Figure 10. Calculated spin density distribution for the ground quintet spin configuration of **1**. Blue and yellow contours represent positive and negative spin densities, respectively. The isodensity surface corresponds to a value of 0.0025 e $bohr^{-3}$.

from the t_{2g}(Fe)−t_{2g}(Mn) net overlap, competing with the above-mentioned ferromagnetic contribution. This could result in an overall antiferromagnetic coupling, as observed in the $Fe^{III}_2Mn^{II}_2$ compound (**1**). In this compound, the ferromagnetic contribution decreases with the bending of the Fe−C−N−M unit (see Table 9).

Finally, in the case of the $Fe^{III}_2Co^{II}_2$ compound (**3b**), the fact that only one t_{2g} magnetic orbital [versus three of them in the manganese(II) ion] is operative for the cobalt(II), ion decreases the antiferromagnetic contributions and then, the ferromagnetic one becomes dominant (see Table 9).

CONCLUSION

In this work, we have described the syntheses, crystallographic structures, and magnetic properties of a new family of heterobimetallic tetranuclear cyanide-bridged complexes of general formula $[Fe^{III}_2M^{II}_2]$ [M = Mn, Ni, and Co] that has been rationally prepared following a molecular-programmed approach consisting of using the tricyanidometalate precursor $[Fe^{III}(L)(CN)_3]^{3-}$ as ligand versus the metal ions [Mn (**1**), Ni (**2a** and **2b**), and Co (**3a** and **3b**)] with four blocked coordination positions by two bidentate imine terminal ligands [bpy (**1**), dmphen (**2a**−**3b**)] forming cyclic tetranuclear structures. This approach is not new but contrasts with the vast majority of previously reported cyanido-bridged tetranuclear squares prepared in a one-pot reaction by serendipitous self-assembly processes. The magnetic coupling between the Fe(III) and M(II) ions through the cyanide bridge is found to be ferromagnetic for M = Ni (**2a** and **2b**) and Co (**3a** and **3b**) and antiferromagnetic for M = Mn (**1**). The nature of these interactions has been rationalized by means of theoretical calculations. Despite the fact that relatively high spin ground states have been obtained in a controlled manner for this family of tetranuclear compounds, [S = 4 (**1**), S = 3 (**2a**, **2b**), and S = 4 (**3a**, **3b**)] with metal ions having a large local magnetic anisotropy such as cobalt(II), no slow magnetic relaxation effects found in single-molecule magnets were observed. However, the rational design of discrete molecules reported herein with a predetermined magnetic behavior opens new gates for the synthesis of novel single-molecule magnets by inserting metal ions with a larger magnetic anisotropy or by better controlling the intermolecular interactions.

ASSOCIATED CONTENT

Supporting Information. Figures S1, S2, and S3 show crystal packing views of **1**, **2b**, and **3b**, respectively. This material is available free of charge via the Internet at http://pubs.acs.org. Crystallographic data (excluding structure factors) for the structures reported in this paper have been deposited with the Cambridge Crystallographic Data Centre as supplementary publication numbers CCDC-815318 (**1**), CCDC-815317 (**2a**), CCDC-7815316 (**2b**), CCDC-815314 (**3a**), and CCDC−815315 (**3b**). Copies of the data can be obtained free of charge on application to CCDC, 12 Union Road, Cambridge CB2 1EZ, U.K. (fax: (+44) 1223 336 033; e-mail: deposit@ccdc.cam.ac.uk).

AUTHOR INFORMATION

Corresponding Author

*E-mail: Rodrigue.Lescouezec@upmc.fr (R.L.).

ACKNOWLEDGMENT

This work was supported by the CNRS (France), the Ministère de l'Enseignement Supérieur et de la Recherche (MESR, France), the MEC (Spain) (Projects CTQ2010-15364, CSD2007-00010, MAT2007-60660, and CSD2006-00015), and the European Union through the Magmanet Network of Excellence (Contract No. 515767-2). E.P. thanks the MEC for a postdoctoral grant.

REFERENCES

(1) (a) Fujita, M. *Acc. Chem. Res.* **1999**, *32*, 53. (b) Fujita, M.; Umemoto, K.; Yoshizawa, M.; Fujita, M.; Kusukawa, T.; Biradha, K. *Chem. Commun.* **2001**, 509.

(2) (a) Albrecht, M. *Chem. Soc. Rev.* **1998**, *27*, 281. (b) Albrecht, M.; Janser, I.; Fröhlich, R. *Chem. Commun.* **2005**, 157.

(3) (a) Caulder, D. L.; Raymond, K. N. *J. Chem. Soc., Dalton Trans.* **1999**, 1185. (b) Fiedler, D.; Leung, D. H.; Bergman, R. G.; Raymond, K. N. *Acc. Chem. Res.* **2005**, *38*, 351.

(4) (a) Thompson, L. K. *Coord. Chem. Rev.* **2002**, *233*−*234*, 193. (b) Dawe, L. N.; Abedin, T. S. M.; Thompson, L. K. *Dalton Trans.* **2008**, 1661.

(5) (a) Lehn, J. M. *Angew. Chem., Int. Ed.* **2004**, *43*, 3644. (b) Ruben, M.; Lehn, J. M.; Müller, P. *Chem. Soc. Rev.* **2006**, *35*, 1056.
(6) Swiegers, G. F.; Malefetse, T. J. *Chem. Rev.* **2000**, *100*, 3483.
(7) Gatteschi, D.; Caneschi, A.; Pardi, L.; Sessoli, R. *Science* **1994**, *265*, 1054.
(8) (a) Sessoli, R.; Gatteschi, D.; Caneschi, A.; Novak, M. A. *Nature* **1993**, *365*, 141. (b) Friedman, J. R.; Sarachik, M. P.; Tejada, J.; Ziolo, R. *Phys. Rev. Lett.* **1996**, *76*, 3830.
(9) Taft, K. L.; Delfs, C. D.; Papaefthymiou, G. C.; Forner, S.; Gatteschi, D.; Lippard, S. J. *J. Am. Chem. Soc.* **1994**, *116*, 823.
(10) (a) Waldmann, O.; Hassmann, J.; Müller, P.; Hanan, G. S.; Volkmer, D.; Schubert, U. S.; Lehn, J. M. *Phys. Rev. Lett.* **1997**, *79*, 3390. (b) Waldmann, O.; Zhao, L.; Thompson, L. K. *Phys. Rev. Lett.* **2002**, *88*, 066401.
(11) (a) Beltran, L. M. C.; Long, J. R. *Acc. Chem. Res.* **2005**, *38*, 325. (b) Beauvais, L. G.; Long, J. R. *J. Am. Chem. Soc.* **2002**, *124*, 12096. (c) Berben, L. A.; Long, J. R. *J. Am. Chem. Soc.* **2002**, *124*, 11588. (d) Sokol, J. J.; Hee, A. G.; Long, J. R. *J. Am. Chem. Soc.* **2002**, *124*, 7656. (e) Shores, M. P.; Sokol, J. J.; Long, J. R. *J. Am. Chem. Soc.* **2002**, *124*, 2279. (f) Beauvais, L. G.; Long, J. R. *J. Am. Chem. Soc.* **2002**, *124*, 2110. (g) Sokol, J. J.; Shores, M. P.; Long, J. R. *Inorg. Chem.* **2002**, *41*, 3052. (h) Sokol, J. J.; Shores, M. P.; Long, J. R. *Angew. Chem., Int. Ed.* **2001**, *40*, 236. (i) Berseth, P. A.; Sokol, J. J.; Shores, M. P.; Heinrich, J. L.; Long, J. R. *J. Am. Chem. Soc.* **2000**, *122*, 9655. (j) Larionova, J.; Gross, M.; Pilkington, M.; Andres, H.; Stoeckli-Evans, H.; Güdel, H. U.; Decurtins, S. *Angew. Chem., Int. Ed.* **2000**, *39*, 1605. (k) Chen, X. Y.; Shi, W.; Xia, J.; Cheng, P.; Zhao, B.; Song, H. B.; Wang, H. G.; Yan, S. P.; Liao, D. Z.; Jiang, Z. H. *Inorg. Chem.* **2005**, *44*, 4263. (l) Ni, Z. H.; Kou, H. Z.; Zhao, Y. H.; Wang, R. J.; Cui, A. L.; Sato, O. *Inorg. Chem.* **2005**, *44*, 2050. (m) Choi, H. J.; Sokol, J. J.; Long, J. R. *Inorg. Chem.* **2004**, *43*, 1606.
(12) (a) Hatlevik, O.; Buschmann, W. E.; Zhang, J.; Manson, J. L.; Miller, J. S. *Adv. Mater.* **1999**, *11*, 914. (b) Holmes, S. M.; Girolami, G. S. *J. Am. Chem. Soc.* **1999**, *121*, 5593. (c) Lu, T. B.; Xiang, H.; Su, C. Y.; Cheng, P.; Mao, Z. W.; Ji, L. N. *New J. Chem.* **2001**, *25*, 216. (d) Inoue, K.; Imai, H.; Chalsasi, P. S.; Kikuchi, K.; Ohba, M.; Ôkawa, H.; Yakhmi, J. V. *Angew. Chem., Int. Ed.* **2001**, *40*, 4242. (e) Kou, H. Z.; Gao, S.; Zhang, J.; Wen, G. H.; Su, G.; Zheng, R. K.; Zhang, X. X. *J. Am. Chem. Soc.* **2001**, *123*, 11809. (f) Dong, W.; Zhu, L. N.; Song, H. B.; Liao, D. Z.; Jiang, Z. H.; Yan, S. P.; Cheng, P.; Gao, S. *Inorg. Chem.* **2004**, *43*, 2465. (g) Ohba, M.; Usuki, N.; Fukita, N.; Ôkawa, H. *Angew. Chem., Int. Ed.* **1999**, *38*, 1795. (h) Tanase, S.; Tuna, F.; Guionneau, P.; Maris, T.; Rombaut, G.; Mathonière, C.; Andruh, M.; Kahn, O.; Sutter, J. *Inorg. Chem.* **2003**, *42*, 1625. (i) Shores, M. P.; Beauvais, L. G.; Long, J. R. *J. Am. Chem. Soc.* **1999**, *121*, 775.
(13) (a) Ferlay, S.; Mallah, T.; Ouahes, R.; Veillet, P.; Verdaguer, M. *Nature* **1995**, *378*, 701.
(14) (a) Li, D.; Clérac, R.; Roubeau, O.; Harté, E.; Mathonière, C.; Le Bris, R.; Holmes, S. M. *J. Am. Chem. Soc.* **2008**, *130*, 252. (b) Zhang, Y.; Li, D.; Clérac, R.; Kalisz, M.; Mathoniére, C.; Holmes, S. *Angew. Chem., Int. Ed.* **2010**, *49*, 3752. (c) Mercurol, J.; Li, Y.; Pardo, E.; Risset, O.; Seuleiman, M.; Rousselière, H.; Lescouëzec, R.; Julve, M. *Chem. Commun.* **2010**, *46*, 8995. (d) Sato, O. *Acc. Chem. Res.* **2003**, *36*, 692–700 and references therein. (e) Arimoto, Y.; Ohkoshi, S.; Zhong, Z. J.; Seino, H.; Mizobe, Y.; Hashimoto, K. *J. Am. Chem. Soc.* **2003**, *125*, 9240.
(15) (a) Nihei, M.; Ui, M.; Yokota, M.; Han, L. Q.; Maeda, A.; Kishida, H.; Okamoto, H.; Oshio, H. *Angew. Chem., Int. Ed.* **2005**, *44*, 6484. (b) Berlinguette, C. P.; Dragulescu-Andrasi, A.; Sieber, A.; Galán-Mascarós, J. R.; Güdel, H.-U.; Achim, C.; Dunbar, K. R. *J. Am. Chem. Soc.* **2004**, *126*, 6222.
(16) Ohkoshi, S.; Tokoro, H.; Matsuda, T.; Takahashi, H.; Irie, H.; Hashimoto, K. *Angew. Chem., Int. Ed.* **2007**, *46*, 3238.
(17) (a) Li, D. F.; Parkin, S.; Wang, G. B.; Yee, G. T.; Prosvirin, A. V.; Holmes, S. M. *Inorg. Chem.* **2005**, *44*, 4903. (b) Sokol, J. J.; Hee, A. G.; Long, J. R. *J. Am. Chem. Soc.* **2002**, *124*, 7656. (c) Choi, H. J.; Sokol, J. J.; Long, J. R. *Inorg. Chem.* **2004**, *43*, 1606. (d) Berlinguette, C. P.; Vaughn, D.; Cañada-Vilalta, C.; Galán-Mascarós, J. R.; Dunbar, K. R. *Angew. Chem., Int. Ed.* **2003**, *42*, 1523–1526. (e) Wang, S.; Zou, J.-L.; Zhou, H.-C.; Choi, H. J.; Ke, Y.; Long, J. R.; You, X.-Z. *Angew. Chem., Int. Ed.* **2004**, *43*, 5940. (f) Schelter, E. J.; Prosvirin, A. V.; Dunbar, K. R. *J. Am. Chem. Soc.* **2004**, *126*, 15004. (g) Pardo, E.; Morales-Osorio, I.; Julve, M.; Lloret, F.; Cano, J.; Ruiz-García, R.; Pasán, J.; Ruiz-Pérez, C.; Ottenwaelder, X.; Journaux, Y. *Inorg. Chem.* **2004**, *43*, 7594.
(18) (a) Lescouëzec, R.; Vaissermann, J.; Ruiz-Pérez, C.; Lloret, F.; Carrasco, R.; Julve, M.; Verdaguer, M.; Dromzee, Y.; Gatteschi, D.; Wernsdorfer, W. *Angew. Chem., Int. Ed.* **2003**, *42*, 1483. (b) Toma, L. M.; Lescouezec, R.; Lloret, F.; Vaissermann, J.; Verdaguer, M. *Chem. Commun.* **2003**, 1850. (c) Toma, L.; Lescouëzec, R.; Pasán, J.; Ruiz-Pérez, C.; Vaissermann, J.; Cano, J.; Carrasco, R.; Wernsdorfer, W.; Lloret, F.; Julve, M. *J. Am. Chem. Soc.* **2006**, *128*, 4842. (d) Toma, L.; Lescouëzec, R.; Uriel, S.; Llusar, R.; Ruiz-Pérez, C.; Vaissermann, J.; Lloret, F.; Julve, M. *Dalton Trans.* **2007**, 3690. (e) Lescouëzec, R.; Toma, L.; Vaissermann, J.; Verdaguer, M.; Delgado, F. S.; Ruiz-Pérez, C.; Lloret, F.; Julve, M. *Coord. Chem. Rev.* **2005**, *249*, 2691–2729. (f) Wang, S.; Zuo, J.-L.; Gao, S.; Song, Y.; Zhou, H.-C.; Zhang, Y.-Z.; You, X.-Z. *J. Am. Chem. Soc.* **2004**, *126*, 8900.
(19) Sessoli, R.; Tsai, H.; Schake, A. R.; Wang, S.; Vincent, J. B.; Folting, K.; Gattechi, D.; Christou, G.; Hendrickson, D. N. *J. Am. Chem. Soc.* **1993**, *115*, 1804.
(20) (a) Caneschi, A.; Gatteschi, D.; Lalioti, N.; Sangregorio, C.; Sessoli, R.; Venturi, G.; Vindigni, A.; Rettori, A.; Pini, M. G.; Novak, M. A. *Angew. Chem., Int. Ed.* **2001**, *40*, 1760. (b) Caneschi, A.; Gatteschi, D.; Lalioti, N.; Sessoli, R.; Sorace, L.; Tanngoulis, V.; Vindigni, A. *Chem.—Eur. J.* **2002**, *8*, 286. (c) Caneschi, A.; Gatteschi, D.; Lalioti, N.; Sangregorio, C.; Sessoli, R.; Venturi, G.; Vindigni, A.; Rettori, A.; Pini, M. G.; Novak, M. A. *Europhys. Lett.* **2002**, *58*, 771. (d) Bogani, L.; Caneschi, A.; Fedi, M.; Gatteschi, D.; Massi, M.; Novak, M. A.; Pini, M. G.; Rettori, A.; Sessoli, R.; Vindigni, A. *Phys. Rev. Lett.* **2004**, *92*, 207204. (e) Clérac, R.; Miyasaka, H.; Yamashita, M.; Coulon, C. *J. Am. Chem. Soc.* **2002**, *124*, 12387. (f) Miyasaka, H.; Clerac, R.; Mizushima, K.; Sugiura, K.; Yamashita, M.; Wernsdorfer, W.; Coulon, C. *Inorg. Chem.* **2003**, *42*, 8203. (g) Miyasaka, H.; Julve, M.; Clérac, R. *Inorg. Chem.* **2009**, *48*, 3420.
(21) (a) Winpenny, R. E. P. *Adv. Inorg. Chem.* **2001**, *52*, 1. (b) Gatteschi, D.; Sessoli, R. *Angew. Chem., Int. Ed.* **2003**, *42*, 268. (c) Gatteschi, D.; Sessoli, R.; Villain, J. *Molecular Nanomagnets*; Oxford University Press: New York, 2006.
(22) Pardo, E.; Ruiz-García, R.; Cano, J.; Ottenwaelder, X.; Lescouëzec, R.; Journaux, Y.; Lloret, F.; Julve, M. *Dalton Trans.* **2008**, 2780.
(23) (a) Kim, J.; Han, S.; Cho, I.-K.; Choi, K. Y.; Heu, M.; Yoon, S.; Suh, B. J. *Polyhedron* **2004**, *23*, 1333–1339. (b) Toma, L. M.; Lescouëzec, R.; Cangussu, D.; Llusar, R.; Mata, J.; Spey, S.; Thomas, J. A.; Lloret, F.; Julve, M. *Inorg. Chem. Commun.* **2005**, *8*, 382. (c) Li, D.; Parkin, S.; Wang, G.; Yee, G. T.; Holmes, S. M. *Inorg. Chem.* **2006**, *45*, 2773. (d) Nihei, M.; Ui, M.; Oshio, H. *Polyhedron* **2009**, *28*, 1718. (e) Karadas, F.; Schelter, E. J.; Shatruk, M.; Prosvirin, A. V.; Bacsa, J.; Smirnov, D.; Ozarowski, J.; Krzystek, A.; Telser, J.; Dunbar, K. R. *Inorg. Chem.* **2008**, *47*, 2074–2082 and references therein. (f) Li, D.; Parkin, S.; Wang, G.; Yee, G. T.; Holmes, S. M. *Inorg. Chem.* **2006**, *45*, 2773–2775. (g) *Progress in Inorganic Chemistry*; Karlin, D., Ed.; Wiley: New York, 2009; Vol. 56.
(24) (a) Lescouëzec, R.; Vaissermann, J.; Lloret, F.; Julve, M.; Verdaguer, M. *Inorg. Chem.* **2002**, *41*, 5943–5945. (b) Li, D.; Clérac, R.; Parkin, S.; Wang, G.; Yee, G. T.; Holmes, S. M. *Inorg. Chem.* **2006**, *45*, 5251–5253.
(25) (a) Becke, A. D. *Phys. Rev. A* **1988**, *38*, 3098. (b) Lee, C.; Yang, W.; Parr, R. G. *Phys. Rev. B* **1988**, *37*, 785. (c) Becke, A. D. *J. Chem. Phys.* **1993**, *98*, 5648.
(26) (a) Schaefer, A.; Horn, A.; Ahlrichs, R. *J. Chem. Phys.* **1992**, *97*, 2571. (b) Schaefer, A.; Huber, C.; Ahlrichs, R. *J. Chem. Phys.* **1994**, *100*, 5829.
(27) Frisch, M. J.; Trucks, G. W.; Schlegel, H. B.; Scuseria, G. E.; Robb, M. A.; Cheeseman, J. R.; Scalmani, G.; Barone, V.; Mennucci, B.; Petersson, G. A.; Nakatsuji, H.; Caricato, M.; Li, X.; Hratchian, H. P.; Izmaylov, A. F.; Bloino, J.; Zheng, G.; Sonnenberg, J. L.; Hada, M.; Ehara, M.; Toyota, K.; Fukuda, R.; Hasegawa, J.; Ishida, M.; Nakajima, T.; Honda, Y.; Kitao, O.; Nakai, H.; Vreven, T.; Montgomery, J. A., Jr.;

Peralta, J. E.; Ogliaro, F.; Bearpark, M.; Heyd, J. J.; Brothers, E.; Kudin, K. N.; Staroverov, V. N.; Kobayashi, R.; Normand, J.; Raghavachari, K.; Rendell, A.; Burant, J. C.; Iyengar, S. S.; Tomasi, J.; Cossi, M.; Rega, N.; Millam, N. J.; Klene, M.; Knox, J. E.; Cross, J. B.; Bakken, V.; Adamo, C.; Jaramillo, J.; Gomperts, R.; Stratmann, R. E.; Yazyev, O.; Austin, A. J.; Cammi, R.; Pomelli, C.; Ochterski, J. W.; Martin, R. L.; Morokuma, K.; Zakrzewski, V. G.; Voth, G. A.; Salvador, P.; Dannenberg, J. J.; Dapprich, S.; Daniels, A. D.; Farkas, Ö.; Foresman, J. B.; Ortiz, J. V.; Cioslowski, J.; Fox, D. J. *Gaussian 09*; Gaussian, Inc.: Wallingford, CT, USA, 2009.

(28) (a) Ruiz, E.; Cano, J.; Alvarez, S.; Alemany, P. *J. Am. Chem. Soc.* **1998**, *120*, 11122. (b) Ruiz, E.; Cano, J.; Alvarez, S.; Alemany, P. *J. Comput. Chem.* **1999**, *20*, 139. (c) Ruiz, E.; Rodríguez-Fortea, A.; Cano, J.; Alvarez, S.; Alemany, P. *J. Comput. Chem.* **2003**, *24*, 982. (d) Ruiz, E.; Cano, J.; Alvarez, S.; Polo, V. *J. Phys. Chem B* **2006**, *110*, 115.

(29) Sarkar, M.; Aromí, G.; Cano, J.; Bertolasi, V.; Ray, D. *Chem.—Eur. J.* **2010**, *16*, 13825.

(30) Visinescu, D.; Toma, L. M.; Cano, J.; Fabelo, O.; Ruiz-Pérez, C.; Labrador, A.; Lloret, F.; Julve, M. *Dalton Trans.* **2010**, *39*, 5028.

(31) Tomasi, J.; Mennucci, B.; Cammi, R. *Chem. Rev.* **2005**, *105*, 2999.

(32) (a) Duisenberg, A. J. M.; Kroon-Batenburg, L. M. J.; Schreurs, A. M. M. *J. Appl. Crystallogr.* **2003**, *36*, 220. (b) Blessing, R. H. *Acta Crystallogr.* **1995**, *A51*, 33. (c) Altomare, A.; Cascarano, G.; Giacomazzo, C.; Guogliardi, A. *J. Appl. Crystallogr.* **1993**, *26*, 343. (d) Palatinus, L.; Chapuis, G. *J. Appl. Crystallogr.* **2007**, *40*, 786. (e) Sheldrick, G. M. *SHELX97, Programs for Crystal Structure Analysis*, release 97-2; Institüt für Anorganische Chemie der Universität Göttingen: Göttingen, Germany, 1998. (f) Betteridge, P. W.; Carruthers, J. R.; Cooper, R. I.; Prout, K.; Watkin, D. J. *J. Appl. Crystallogr.* **2003**, *36*, 1487. (g) Hooft, R. W. W. *COLLECT*; Nonius BV: Delft, The Netherlands, 1999. (h) Farrugia, L. J. *J. Appl. Crystallogr.* **1999**, *32*, 837. (i) Spek, A. L. *J. Appl. Crystallogr.* **2003**, *36*, 7. (j) Palmer, D. *CRYSTAL MAKER*; Cambridge University Technical Services: Cambridge, U.K., 1996.

(33) Cano, J. *VPMAG Package*; University of Valencia: Valencia, Spain, 2003.

(34) Lloret, F.; Julve, M.; Cano, J.; Ruiz-García, R.; Pardo, E. *Inorg. Chim. Acta* **2008**, *361*, 3432. (b) Pardo, E.; Ruiz-García, R.; Lloret, F.; Faus, J.; Julve, M.; Journaux, Y.; Delgado, F. S.; Ruiz-Pérez, C. *Adv. Mater.* **2004**, *16*, 1597. (c) Pardo, E.; Ruiz-García, R.; Lloret, F.; Faus, J.; Julve, M.; Journaux, Y.; Novak, M. A.; Delgado, F. S.; Ruiz-Pérez, C. *Chem.—Eur. J.* **2007**, *13*, 2054. (d) Pardo, E.; Train, C.; Lescouëzec, R.; Journaux, Y.; Pasán, J.; Ruiz-Pérez, C.; Delgado, F. S.; Ruiz-García, R.; Lloret, F.; Paulsen, C. *Chem. Commun.* **2010**, *46*, 2322.

(35) Park, K.; Holmes, S. M. *Phys. Rev. B* **2006**, *74*, 224440.

(36) (a) Toma, L. M.; Delgado, F. S.; Ruiz-Pérez, C.; Carrasco, R.; Cano, J.; Lloret, F.; Julve, M. *Dalton Trans.* **2004**, 2836. (b) Toma, L.; Toma, L. M.; Lescouëzec, R.; Armentano, D.; De Munno, G.; Andruh, M.; Cano, J.; Lloret, F.; Julve, M. *Dalton Trans.* **2005**, 1357. (c) Toma, L. M.; Lescouëzec, R.; Vaissermann, J.; Delgado, F. S.; Ruiz-Pérez, C.; Carrasco, R.; Cano, J.; Lloret, F.; Julve, M. *Chem.—Eur. J.* **2004**, *10*, 6130. (d) Toma, L. M.; Toma, L. D.; Delgado, F. S.; Ruiz-Pérez, C.; Sletten, J.; Cano, J.; Clemente-Juan, J. M.; Lloret, F.; Julve, M. *Coord. Chem. Rev.* **2006**, *250*, 2176. (e) Rodríguez-Diéguez, A.; Kivekas, R.; Sillanpaa, R.; Cano, J.; Lloret, F.; McKee, V.; Stoeckli-Evans, H.; Colacio, E. *Inorg. Chem.* **2006**, *45*, 10537.